LIDAR-MEASURED WIND PROFILES

The Missing Link in the Global Observing System

BY WAYMAN E. BAKER, ROBERT ATLAS, CARLA CARDINALI, AMY CLEMENT, GEORGE D. EMMITT, BRUCE M. GENTRY, R. MICHAEL HARDESTY, ERLAND KÄLLÉN, MICHAEL J. KAVAYA, ROLF LANGLAND, ZAIZHONG MA, MICHIKO MASUTANI, WILL MCCARTY, R. BRADLEY PIERCE, ZHAOXIA PU, LARS PETER RIISHOJGAARD, JAMES RYAN, SARA TUCKER, MARTIN WEISSMANN, AND JAMES G. YOE

Doppler lidar technology has advanced to the point where wind measurements can be made with confidence from space, thus filling a major gap in the global observing system.

The purpose of this paper is to document the advances in our understanding of the need for global wind measurements since our earlier paper (Baker et al. 1995), to summarize recent results from airborne wind measurement campaigns and OSSEs, and to discuss the technology advances that now make a space-based Doppler wind lidar (DWL) feasible.

Measurement of the three-dimensional global wind field is the final frontier that must be crossed to significantly improve the initial conditions for numerical weather forecasts. The World Meteorological Organization determined that global wind profiles are "essential for operational weather forecasting on all scales and at all latitudes." (WMO 1996, chapter 13, p. 295) This is because the wind field plays a unique dynamical role in forcing the mass field to adjust to it at all scales in the tropics, and at small scales in the extratropics (Baker et al. 1995). Wind profiles are also needed to depict vertical wind shear structures that are underrepresented in global NWP models (Houchi et al. 2010). Furthermore, the National Research Council (NRC) decadal survey

AFFILIATIONS: BAKER*—NOAA, McHenry, Maryland; ATLAS—NOAA/Atlantic Oceanographic and Meteorological Laboratory, Miami, Florida; CARDINALI AND KÄLLÉN—European Centre for Medium-Range Weather Forecasts, Reading, United Kingdom; CLEMENT—University of Miami, Miami, Florida; EMMITT—Simpson Weather Associates, Charlottesville, Virginia; GENTRY AND MCCARTY—NASA Goddard Space Flight Center, Greenbelt, Maryland; HARDESTY—Cooperative Institute for Research in Environmental Sciences, University of Colorado at Boulder, Boulder, Colorado; KAVAYA—NASA Langley Research Center, Hampton, Virginia; LANGLAND—Naval Research Laboratory, Monterey, California; RIISHOJGAARD—World Meteorological Organization, Geneva, Switzerland; MA AND YOE—Joint Center for Satellite Data Assimilation, College Park, Maryland; MASUTANI—NOAA/Environmental Modeling Center, College Park, Maryland; PIERCE—NOAA/National Environmental Satellite, Data, and Information Service, Madison, Wisconsin; PU—University of Utah, Salt Lake City, Utah; RYAN—University of New Hampshire, Durham, New Hampshire; TUCKER—Ball Aerospace and Technologies Corp., Boulder, Colorado; WEISSMANN—Hans-Ertel-Centre for Weather Research, Ludwig-Maximilians-Universität München, Munich, Germany
* Retired
CORRESPONDING AUTHOR: Dr. Wayman E. Baker, 253 Gleanings Drive, McHenry, MD 21541
E-mail: wayman.baker@gmail.com

The abstract for this article can be found in this issue, following the table of contents.

DOI:10.1175/BAMS-D-12-00164.1

A supplement to this article is available online (10.1175/BAMS-D-12-00164.2)

In final form 27 August 2013

report on *Earth Science and Applications from Space* (NRC 2007) recommended a global wind mission, and the NRC Weather Panel, in the same report, determined that a DWL in low-Earth orbit (LEO) could make a *transformational* impact on global tropospheric and stratospheric analyses. More recently, a WMO (2012b) workshop found the current global observing systems to be heavily skewed toward measuring atmospheric mass rather than wind, especially for the satellite instruments, even though the average influence of wind observations is higher, on both an individual instrument and a "per observation" basis. The workshop final report further stated, "There is a need to invest in enhanced wind observations in the tropics and over the oceans especially. . . . Development of satellite-based wind-profiling systems remains a priority for the future global observing system" (WMO 2012b, p. 9) In addition, the WMO Rolling Review of Requirements, updated in May 2012, states that "wind profiles at all levels outside the main populated areas" is the highest measurement priority (WMO 2012a, p. 8).

Accurate measurements of the global wind field will also support major advances in the understanding of several key climate change issues. Several studies have suggested that the general circulation of the atmosphere varies considerably on decadal time scales and that some of this variation may be due to greenhouse gas forcing (Chen et al. 2002; Mitas and Clement 2005, 2006; Vecchi et al. 2006). Each of these studies, however, relies on climate models and datasets that provide an incomplete picture of large-scale circulation changes.

Moreover, there is an urgent need to improve the accuracy of horizontal and vertical transport estimates for climate applications. For example, recent studies (Graversen 2006; Graversen et al. 2008) indicate that the dramatic reduction in sea ice extent observed in the Arctic may be partly due to systematic changes to heat transport into the Arctic. In addition, Yang et al. (2010) found that about 50% of the recent Arctic warming in the free troposphere is due to increased poleward energy transport. However, these findings are based on reanalysis wind data with large uncertainties in the Arctic for the zonally averaged, meridional wind component.

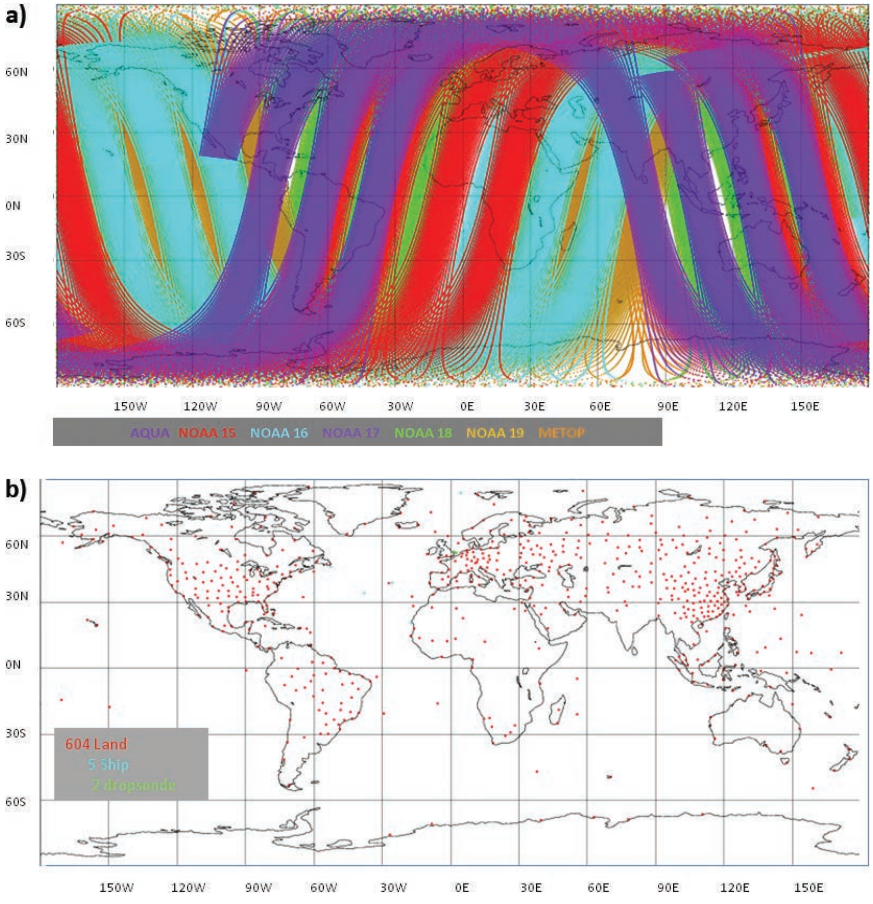

Fig. 1. Depicted is (a) the current upper-air AMSU-measured mass and (b) the 1200 UTC radiosonde-measured wind observational coverage. Maps provided by ECMWF.

Large areas of the tropical atmosphere are devoid of measured wind profiles. This suggests the potential for a large improvement in forecast skill for a variety of tropical phenomena, including tropical cyclones, monsoonal circulations, and the African easterly jet, especially given the dominance of the wind field in the mass–motion balance relationship (Baker et al. 1995; Žagar et al. 2008).

The scientific evidence thus supports the notion of a clear imbalance in the current global observing system as noted above (WMO 2012b). A comparison of atmospheric mass field measurements coverage by satellites in LEO versus the coverage of the radiosonde network is striking. The radiosonde

network, which is primarily land based, remains the primary source of global wind profiles. While single-level wind measurements obtained from aircraft, by tracking cloud or water vapor features from scatterometers, etc., are important components of the global observing system, additional wind profiles are needed, especially over the oceans and remote land areas to depict vertical wind shear structures as noted above (Houchi et al. 2010).

Figure 1 illustrates the measurement imbalance between the mass and wind fields by comparing the coverage of seven Advanced Microwave Sounding Units (AMSUs) and the 1200 UTC radiosonde locations where wind profiles are provided, typically twice per day (once per day over some parts of South America and Australia). In addition to AMSU coverage, global mass data are also provided by three hyperspectral sounders [the National Aeronautics and Space Administration (NASA) Atmospheric Infrared Sounder (AIRS), the European Organisation for the Exploitation of Meteorological Satellites (EUMETSAT) Infrared Atmospheric Sounding Interferometer (IASI), and the *Suomi National Polar-Orbiting Partnership* (*NPP*) satellite Cross-Track Infrared Sounder (CrIS)]. Satellite temperature profiles are also obtained via the Taiwan–United States Constellation Observing System for Meteorology, Ionosphere and Climate (COSMIC; Anthes et al. 2008).

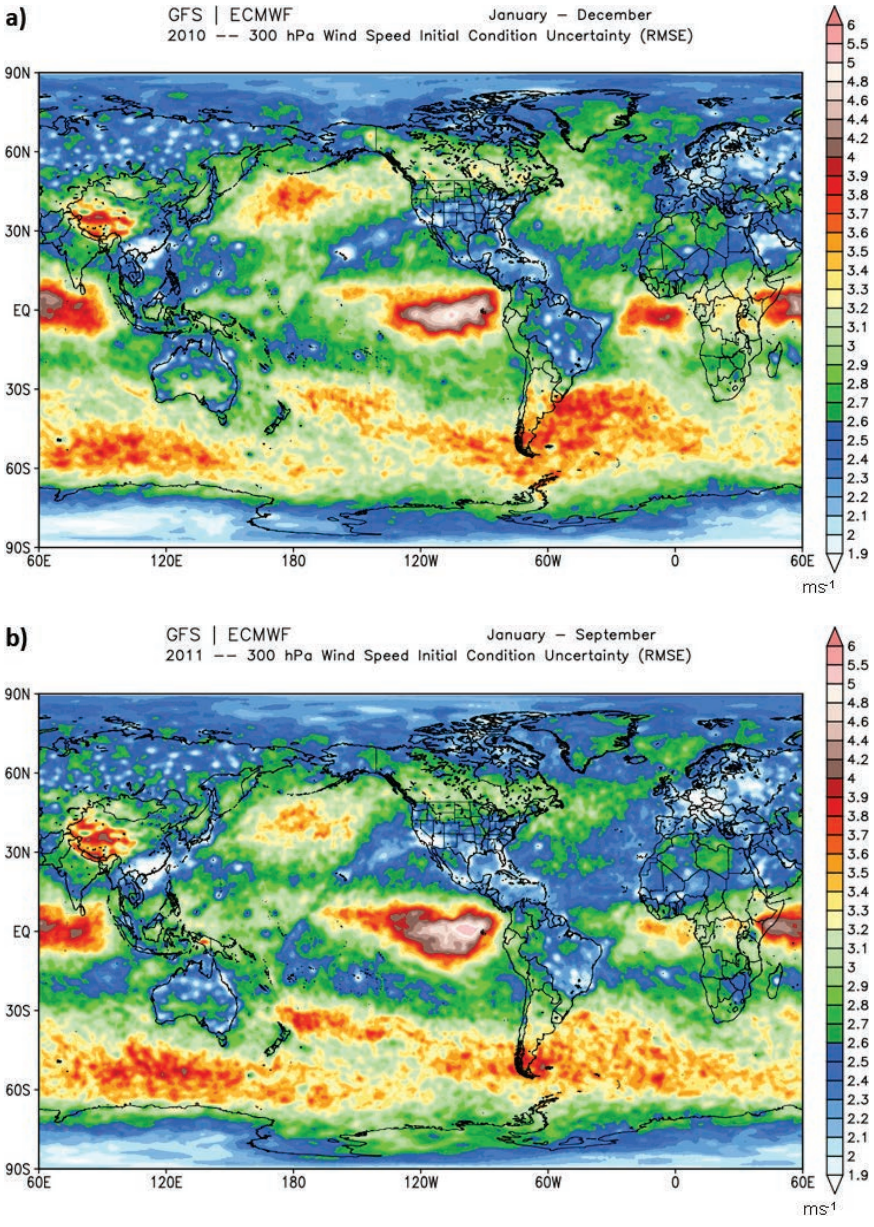

Fig. 2. Depicted are the RMS differences (m s^{-1}) in 300-hPa wind speed analyses produced by ECMWF and the NCEP GFS: (a) Jan–Dec 2010 and (b) Jan–Sep 2011. Includes all daily analyses provided at 0000 and 1200 UTC. This quantity is a proxy for actual analysis error, which cannot be directly quantified. Note that the influence of individual radiosonde stations appears in many areas (Russia, Australia, Brazil, and oceanic islands) as localized regions of reduced analysis difference. Effect of aircraft observations can also be seen [e.g., along the flight corridor between Hawaii and the West Coast (Langland and Maue 2012)].

One measure of the uncertainty of atmospheric analyses is the difference between analyses produced by various operational data assimilation systems, such as those at the European Centre for Medium-Range Weather Forecasts (ECMWF) and National Centers for Environmental Prediction (NCEP). These analysis differences are estimates of actual analysis error, which cannot be directly quantified because the true atmospheric state at any given time is unknown. We show results obtained as multimonth averages

during 2010 (Fig. 2a) and 2011 (Fig. 2b) in o rder to demonstrate that the basic pattern of these differences is quite robust from year to year, which implies a strong dependence of analysis error on the components and quality of the global observing system. The basic global pattern of analysis differences can be modulated to some extent by year-to-year and seasonal variability in atmospheric circulation, as seen by comparing Figs. 2a,b.

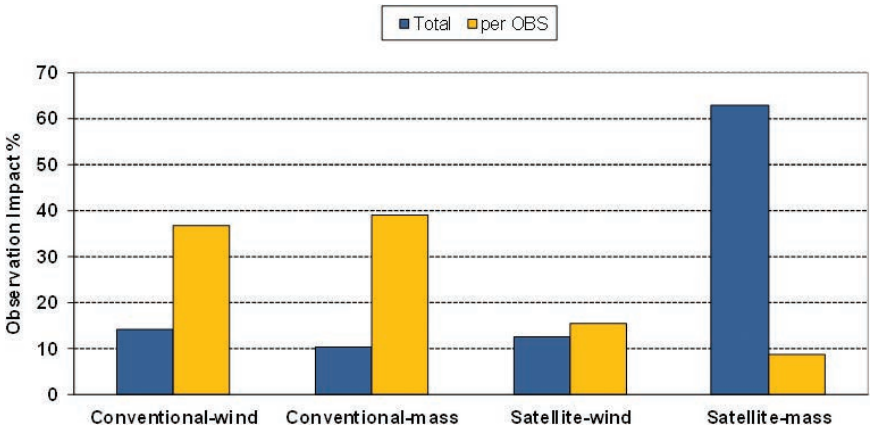

Fig. 3. The contribution of mass vs wind observations in reducing the 24-h forecast error, expressed as observation impact (%), in terms of the total number of observations and on a per-observation basis for the ECMWF data assimilation system.

In regions such as Europe, the United States, and East Asia that are well covered by radiosonde, aircraft, and land surface observations, the differences between ECMWF and NCEP analyses of upper-tropospheric winds (Figs. 2a,b) are relatively small, with correspondingly small analysis uncertainty. Similar patterns exist in the lower troposphere for variables such as temperature and geopotential height (Langland et al. 2008). In contrast, in regions where atmospheric analyses rely primarily on satellite radiance data, there tend to be larger differences between the various analyses of wind, temperature, and height, indicative of larger analysis uncertainties. For example, in Figs. 2a,b there is larger uncertainty in the analyzed 300-hPa wind speed over much of the tropics, southern midlatitudes, and North Pacific basin. Wind observations from geostationary satellite imagery reduce analysis uncertainty but not to the same extent as do observations from radiosondes. Note that analysis uncertainty is smaller over the North Atlantic than over the North Pacific due to more numerous aircraft observations. Analysis differences in polar regions are also generally somewhat smaller due to the prevailing wind–mass balance and the availability of Moderate Resolution Imaging Spectroradiometer (MODIS) and Advanced Very High Resolution Radiometer (AVHRR) wind observations (Key et al. 2003).

IMPACT OF GLOBAL WIND PROFILES ON WEATHER FORECASTING AND CLIMATE RESEARCH.

NWP. Forecast sensitivity to observations. The relative impact of various types of measurements on the quality of atmospheric analyses can be estimated by the so-called forecast sensitivity to observations (FSO), developed by Baker (2000). The FSO technique has been used extensively to assess the sensitivity of forecast errors to different components of the global observing system (Baker and Langland 2008, 2009; Cardinali 2009; Gelaro et al. 2010; Langland and Baker 2004; Ota et al. 2013). This approach can also be used to assess the relative influence of mass and wind field observations on short-range forecast errors.

In Fig. 3 (Källén et al. 2010), the forecast error impact is given for the total number of observations of each type, as well as the error contribution per observation for the ECMWF data assimilation system. As may be seen in Fig. 3, the conventional observing system is well balanced in terms of mass and wind observations, while the satellite observing system is dominated by mass observations. If, however, the impact factor is divided by the number of observations, the individual space-based wind observations are more influential than the space-based mass observations. This evidence is further confirmation that the space-based observing system is unbalanced in terms of the total number of mass and wind observations, as discussed above, but the available wind observations still have a large impact on forecast quality.

OSSEs. An extensive series of global observing system simulation experiments (OSSEs) has been conducted since the mid-1980s to determine the potential influence of wind profile observations from space and to evaluate trade-offs in the design of a space-based wind lidar. These early experiments showed the great potential for space-based wind profile observations reducing analysis errors and improving numerical

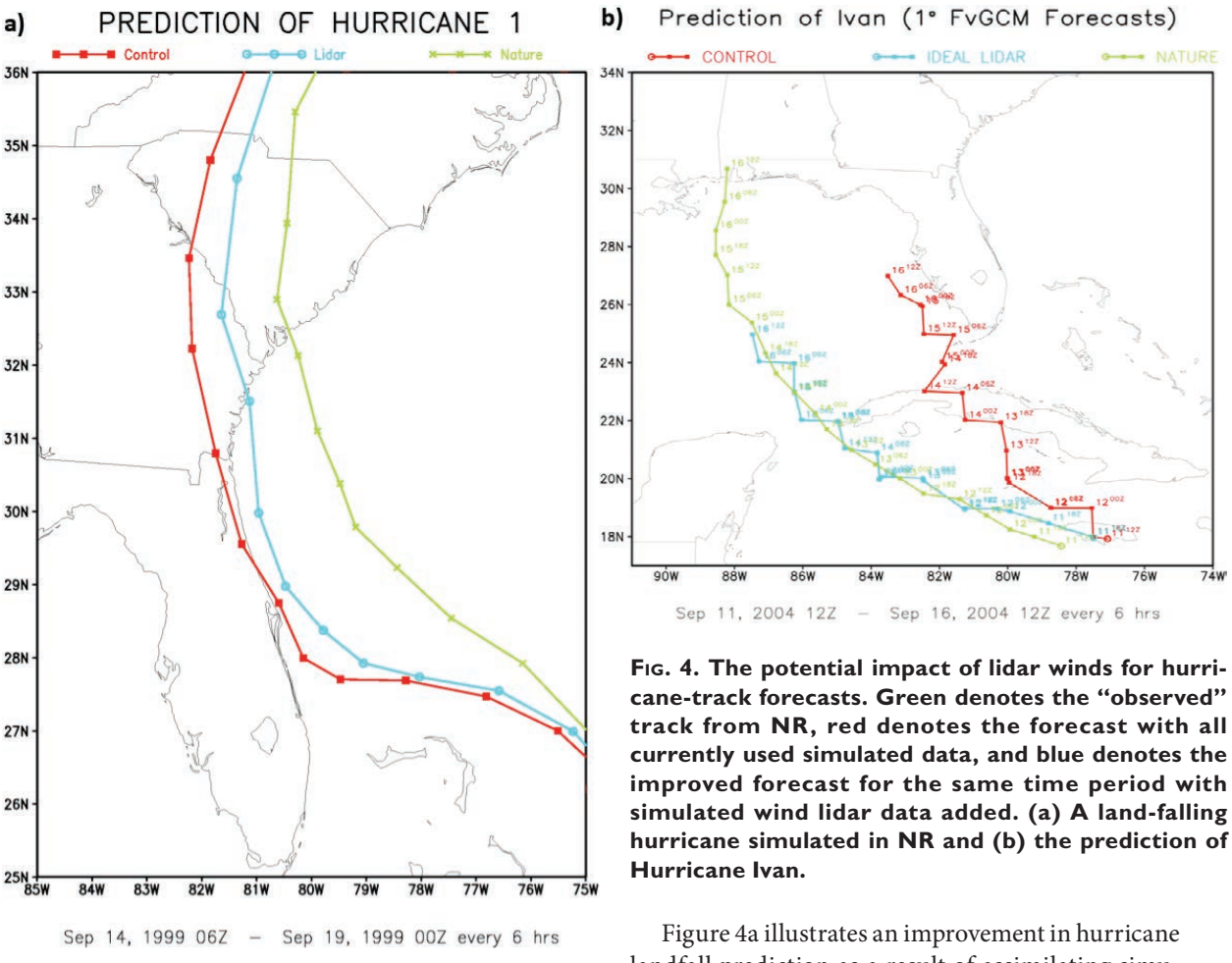

Fig. 4. The potential impact of lidar winds for hurricane-track forecasts. Green denotes the "observed" track from NR, red denotes the forecast with all currently used simulated data, and blue denotes the improved forecast for the same time period with simulated wind lidar data added. (a) A land-falling hurricane simulated in NR and (b) the prediction of Hurricane Ivan.

forecasts. These studies were also used to evaluate trade-offs in lidar design (Atlas et al. 1985a,b; Atlas 1997; Masutani et al. 2010).

OSSEs have also been used to assess the potential impact of DWL on hurricane-track forecasts. For this purpose, a reference atmosphere, referred to as a "nature run" (NR), was generated using an early version of the finite-volume general circulation model (FvGCM) at 0.5° resolution (Atlas et al. 2005b), and the assimilation and forecast system was the 1.0° resolution version of the NASA Goddard Space Flight Center (GSFC) Goddard Earth Observing System (GEOS) version 3 data assimilation system (Atlas et al. 2005a). The NR covered a 3.5-month period and contained interesting and important meteorological features, including tropical cyclones and a very realistic representation of atmospheric fronts and extratropical cyclone evolution. Following a detailed assessment of the realism of the NR and the differences between the NR model and the assimilation–forecasting model, the entire OSSE system was validated through a comparison of parallel real-data and simulated-data impact experiments.

Figure 4a illustrates an improvement in hurricane landfall prediction as a result of assimilating simulated lidar wind data. The predicted landfall position error was improved by approximately 150 miles. Details of these and other OSSEs are summarized by Atlas and Emmitt (2008) and Atlas and Riishojgaard (2008). Marseille et al. (2008) used a modified OSSE concept to illustrate beneficial DWL impact for severe extratropical storms. Pu et al. (2009) and Zhang and Pu (2010) demonstrated DWL data can have a potential impact on improving tropical cyclone intensity forecasts with a regional OSSE.

A second U.S. landfalling storm (Hurricane Ivan) was evaluated from the extremely active 2004 hurricane season. A "QuickOSSE" methodology was conceived in order to answer observational and dynamical questions related to this hurricane. This methodology involved using a 0.25° resolution version of the FvGCM forecast of Hurricane Ivan for the NR. From this NR, all of the standard and special reconnaissance observations that were available in real time, as well as hypothetical lidar wind profiles covering the storm, were simulated. This was followed by the control assimilation and forecast (using all of the standard observations) and an ideal lidar

assimilation and forecast (adding simulated lidar winds to the control) generated using a coarse 1.0° × 1.25° resolution version of the FvGCM.

Figure 4b shows a major improvement in the predicted movement of the hurricane resulting from the assimilation of lidar winds. This was due to a significant improvement in the divergence profile associated with the storm (not shown), enabling it to be more accurately steered by the large-scale flow.

More recently, an ECMWF T511 (~40-km horizontal resolution) NR (Andersson and Masutani 2010) was used to create the simulated observations and serve as the "truth" for impact experiment verification. The Joint Center for Satellite Data Assimilation (JCSDA) has conducted a series of OSSEs aimed at assessing the potential impact of the Global Wind Observing System (GWOS) mission concept outlined in the "Technology used in DWL" section (Riishojgaard et al. 2012), using the T511 nature run provided by ECMWF. All experiments were done with the December 2009 version of the NCEP Global Data Assimilation System (Kleist et al. 2009).

The approach taken to simulate the reference observing system for the OSSEs was simple and aimed at capturing the most salient characteristics of the global observing system. For data with existing real-data parallels (i.e., radiosondes, surface observations, aircraft data, existing satellite systems), simulated observations were created at the times and locations for which actual observations were available in the corresponding 2005–06 period, as recorded in the operational data stream used in NCEP operations. The GWOS DWL observations were simulated, using the Doppler Lidar Simulation Model (DLSM) described by Wood et al. (2000). Direct and coherent detection wind lidar returns (see "Technology used in DWL") were simulated separately, and a detailed model of the instrument error propagation onto the final error of the wind product was included. Details on the simulation of non-DWL data were described by Riishojgaard et al. (2012).

First, a control experiment was performed: a cycling data assimilation run extending over a spinup period from 1 through 6 July, followed by an experimental period from 7 July through 15 August. The control experiment used simulated data for all of the observations with a real-data counterpart in the NCEP operational data stream during this time period that also provided a 40-day interval over which

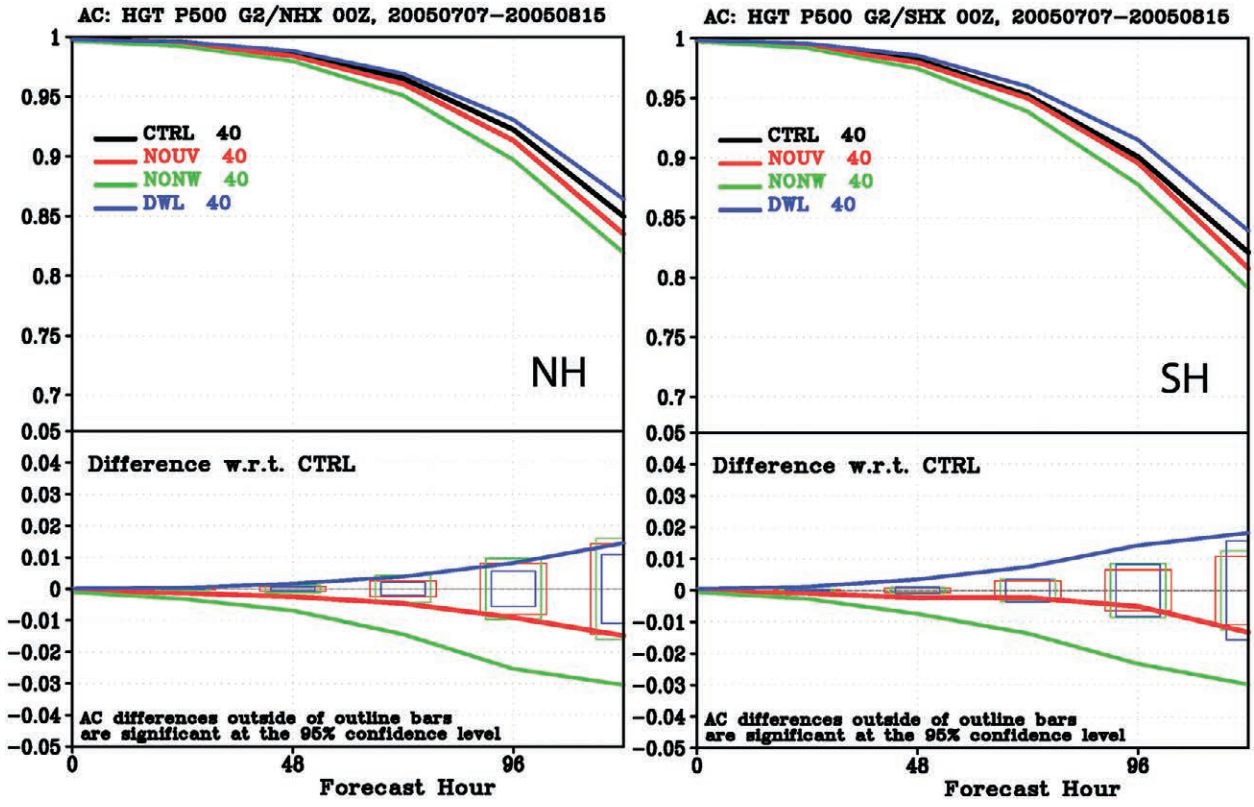

Fig. 5. The impact of various wind observing systems on 500-hPa height forecasts measured by the AC score, averaged over 40 cases. (left) NH and (right) SH results. Error bars represent statistical significance at the 95% level.

diagnostics were calculated. During this period, 5-day forecasts were launched each day at 0000 UTC. Next, a set of three perturbation (assessment) experiments was done: 1) an experiment ("NOUV") from which all radiosonde, pilot balloon, and dropsonde wind observations were removed; 2) an experiment ("NONW") in which all wind observations were withheld (aircraft, scatterometer, winds from feature tracking, etc.) in addition to those withheld from the NOUV experiment (in other words, all wind observations used in the control experiment were withheld.); and 3) an experiment ("DWL") in which the simulated GWOS DWL observations were added to the observations used for the control run. The experimental setup for all runs was consistent with the way the system was used in NCEP operations prior to 22 May 2012. The horizontal resolution was T382, corresponding to a Gaussian grid size of about 45 km.

Figure 5 shows the skill of the 500-hPa-height forecasts as measured by the anomaly correlation coefficient (Miyakoda et al. 1972), referred to here as the anomaly correlation (AC) score, for all four experiments in the Northern Hemisphere (left) and the Southern Hemisphere (right). The AC score can range between 0.0 and 1.0 and is nondimensional. All forecasts were verified using the nature run, and the bottom part of Fig. 5 shows differences in skill with respect to the control run. Differences that exceed the error bars for the respective color are statistically significant at the 95% level. The figure shows that elimination of all wind observations leads to a significant decrease in skill (NOUV and NONW), demonstrating that wind observations have a significant contribution to the skill of the NCEP Global Forecast System (GFS). The addition of the simulated lidar wind observations leads to a statistically significant increase in AC score at day 5 (120 h) of approximately 1.5 and 2 points in the Northern and Southern Hemispheres, respectively. In the Southern Hemisphere, for example, the AC score, is approximately 0.83 versus 0.85 for the control and DWL experiments, respectively.

For comparison purposes, the overall rate of progress of NWP skill over the last 10–20 years has generally ranged from 0.5 to 1 point annually due to a combination of factors: better observations, improvements to model and data assimilation methodology through scientific advances, and increased spatial and temporal resolution due to more powerful computers. Typically, a contribution that can be attributed to a

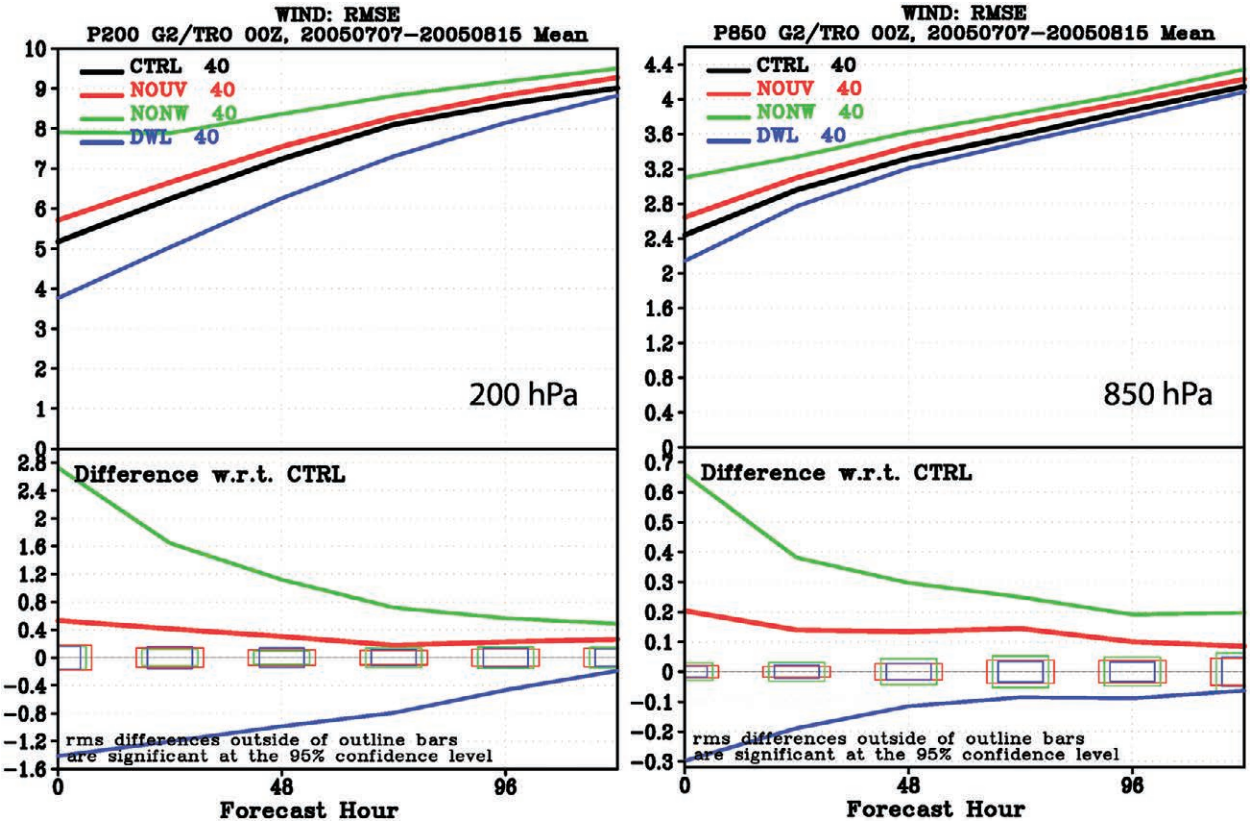

Fig. 6. The impact of various wind-observing systems on 200- and 850-hPa tropical wind forecasts measured by the RMS error (m s^{-1}), averaged over 40 cases. Error bars represent statistical significance at the 95% level.

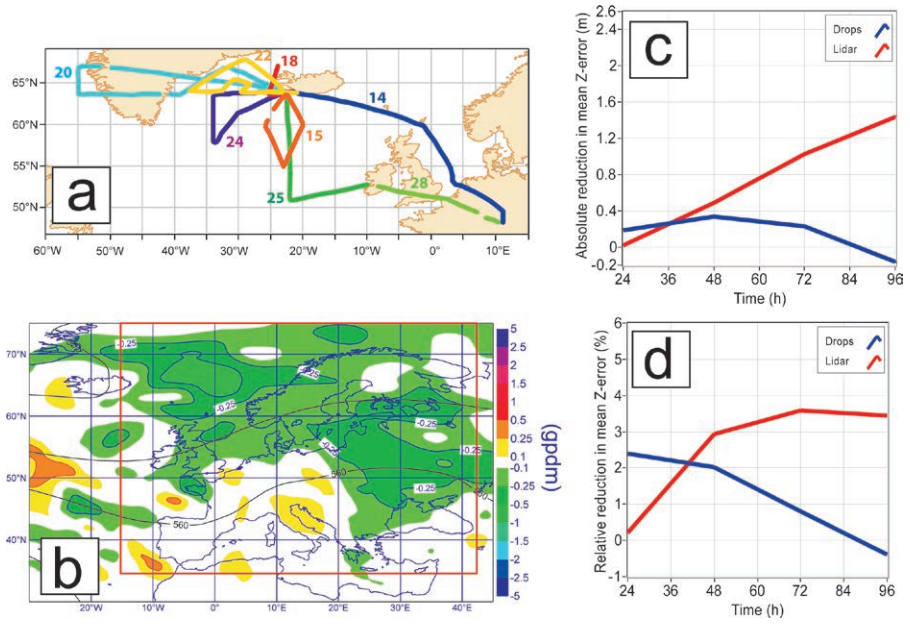

Fig. 7. (a) Flight tracks with lidar observations during the A-TReC. Numbers indicate the day of the flight in Nov 2003. (b) Difference of 500-hPa geopotential height RMS error between an experiment with lidar data and a control run without additional observations. Negative values indicate improvement compared to the control run. (c) Reduction of mean 500-hPa geopotential height errors in an experiment with (red) lidar and (blue) dropsondes compared to the control run. Positive values correspond to lower errors than the control run. (d) As in (c), except normalized with the mean error of the control run.

specific new observing system is generally modest. In that context, the magnitude of the impact of the DWL is exceedingly rare.

Tropical RMS wind errors for the four experiments are shown in Fig. 6. The effect of simulated lidar wind observations in the tropics is initially large, especially at the 200-hPa level. The 850-hPa level is more strongly influenced by the lower boundary conditions and, due to progressive attenuation of the lidar beam at lower levels, fewer wind observations are available at this level. However, the impact tends to decrease rapidly over time at both levels. This behavior is typical for the tropics, and, rather than pointing to problems with the simulated data, it illustrates the challenge of using observations in a dynamically consistent way (Žagar et al. 2004).

Airborne Observing System Experiment over the North Atlantic. A scanning coherent 2-μm Doppler lidar was operated for 28.5 flight hours during the Atlantic "The Observing System Research and Predictability Experiment" (THORPEX) Regional Campaign (A-TReC) in November 2003 onboard the Falcon 20 aircraft of the Deutsches Zentrum für Luft- und Raumfahrt (DLR). The system measured 1612 vertical profiles of wind direction and speed at a resolution of 5–10 km horizontally and 100 m vertically (Fig. 7). Comparison of the lidar observations and collocated dropsondes revealed that the coherent lidar can measure winds with a standard deviation of 0.75–1 m s^{-1} and no significant bias (Weissmann et al. 2005). Although this error is slightly higher than that of conventional dropsonde observations, lidar observations are seen to be more representative of the model wind field because they are computed by averaging over a sampling volume of 5–10 km.

An Observing System Experiment (OSE) was conducted whereby A-TReC lidar observations were assimilated into the operational version of the ECMWF model at that time with a horizontal resolution of about 40 km and 60 levels in the vertical (Weissmann and Cardinali 2007), including the representativeness error. The assumed lidar observation error standard deviation was 1–1.5 m s^{-1}, which is only about half of the assigned error of most conventional observations. Lidar observations were found to have more influence in the analysis than dropsondes. In particular, the mean analysis influence calculated following Cardinali et al. (2004) was 50% higher. The assimilation of lidar wind profiles over the North Atlantic produced an average reduction of 3% in the 48–96-h forecast error for the 500-hPa geopotential height over Europe (Fig. 7). This was a remarkable result given that observations from only eight flights were assimilated in the 17-day period. Consistent with dropsondes having less influence in the analysis, there was less reduction in the forecast error when only dropsonde observations were assimilated (in addition to data from the routine operational observing system).

These findings motivated the deployment of the airborne DWL instruments in the THORPEX Pacific Asian Regional campaign (T-PARC) 2008. Results from this campaign are summarized below.

Airborne OSE over the western Pacific. During the T-PARC field experiment in 2008, airborne DWLs were operated on board the DLR Falcon aircraft and a Naval Research Laboratory (NRL) P-3 aircraft. It was the first time that airborne DWLs were employed for an extended period in the environment of tropical cyclones (TCs). DWL wind measurements were obtained for several TC cases over the western North Pacific. After the field experiment, DLR Falcon DWL observations in the environment of Typhoon Sinlaku were assimilated in the global ECMWF and NRL models. In addition, NRL P-3 DWL observations near Typhoons Nuri and Hagupit were assimilated using the Weather Research and Forecasting Model (WRF).

The DLR Falcon observed over 4000 wind profiles below 9–12 km MSL. About 2500 profiles in an 11-day period covering the life cycle of Typhoon Sinlaku were used in an OSE with the ECMWF and NRL global NWP models. Overall, the DWL observations improved both model forecasts near the observation area (Weissmann et al. 2012). On average, a typhoon track improvement of 9% in the 12–120-h forecast range was obtained with the ECMWF model, with a mean 24–120-h forecast error reduction of 2.5%–5.5% for the 500- and 1000-hPa geopotential height for two verification regions: one area covered the track of Sinlaku and a larger one also included the interaction of Sinlaku with the midlatitudes. In contrast, the NRL experiments did not lead to a significant track improvement likely due to the use of synthetic TC bogus observations that seemed to limit the influence of additional observations near TCs. The mean 24–120-h forecast error of 1000- and 500-hPa geopotential heights, however, was reduced by 1%–3.5% in the same verification areas as with the ECMWF experiments.

Additionally, the DWL observation impact in the ECMWF and NRL models was quantified using FSO diagnostics (Langland and Baker 2004; Cardinali 2009), which confirmed the beneficial impact of DWL observations (Weissmann et al. 2012). The total relative contribution of DWL observations was about twice as high in the NRL system as in the ECMWF system. This is believed to be due to the fewer number of satellite observations assimilated in the NRL system at the time. In the Sinlaku environment and for the NRL system, DWL data had the fourth-largest mean forecast impact per observation, after synthetic TC bogus observations, satellite-derived total precipitable water, and scatterometer surface wind data (Fig. 8a). The impact of DWL measurements in the ECMWF system was similar to that of aircraft observations but smaller than those of drifting buoys, radiosonde and wind profiler observations, atmospheric motion vectors, surface stations, and scatterometer surface winds (Fig. 8b).

A three-dimensional variational data assimilation (3D-Var) WRF system was also used to assimilate the NRL P-3 DWL observations obtained during the early development of Typhoon Nuri, mainly available below 2-km height with 50-m vertical and 1-km horizontal resolution. The P-3 aircraft track and a portion of the path of Nuri in its early development

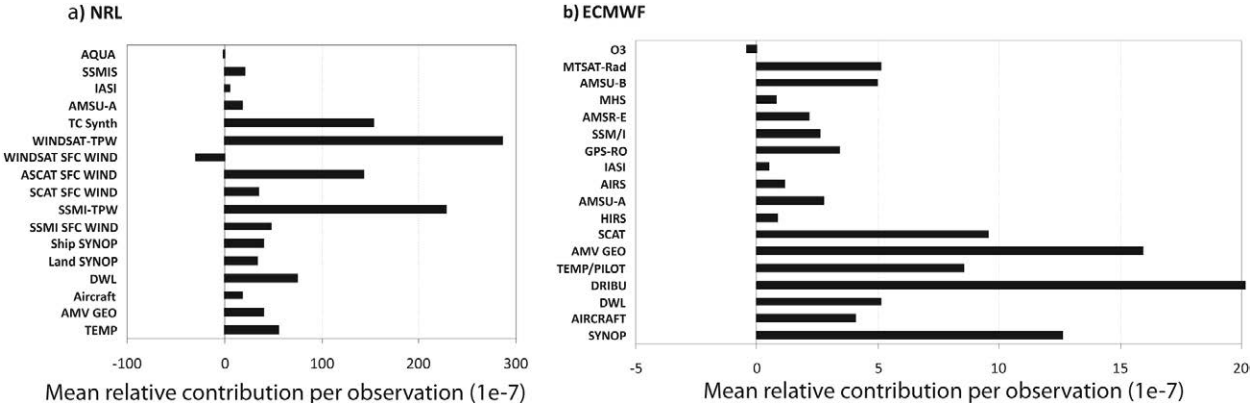

Fig. 8. Mean relative contribution (per observation) of various observation types to the reduction in the 24-h forecast error norm in an area covering Typhoon Sinlaku and its environment (20°–50°N, 120°–160°W) in an experiment with the (a) NRL and (b) ECMWF global models. Scaling is 10^{-7} and positive values represent error reduction. ECMWF results are averaged over all assimilation intervals in the period 11–21 Sep 2008; NRL results only over twelve 6-h assimilation intervals with DWL observations in this period. Contribution of drifting buoy observations in (b) is 63×10^{-7}, which exceeds the scale. Note that the relative magnitude in (a) and (b) should be compared, but not the actual values due to the differences between NRL and ECMWF in the number of observations assimilated, length and number of assimilation intervals, and the "super ob" observation-averaging technique used at NRL. See Weissmann et al. (2012) for more details.

are shown in Fig. 9. Details on the model formulation, the 3D-Var analysis, and initialization procedure can be found in Skamarock et al. (2005), Barker et al. (2004), Pu et al. (2010), and Emmitt et al. (2011a).

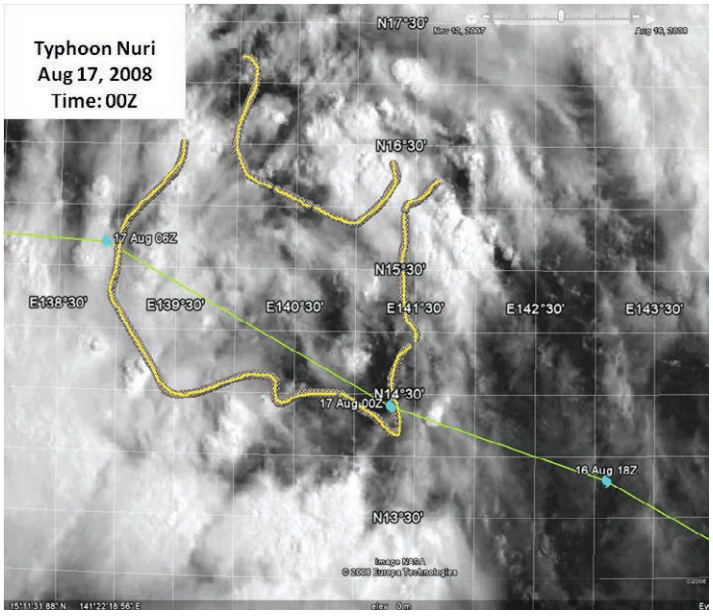

Fig. 9. DWL wind measurements (500 data points collected) at 1500 m above MSL selected from 500 wind profiles around the early stages of Typhoon Nuri (2008) over the western Pacific during 2330 UTC 16 Aug–0200 UTC 17 Aug 2008. NRL P-3 aircraft was flying at 3000 m. Track of Nuri for three 6-h periods is included.

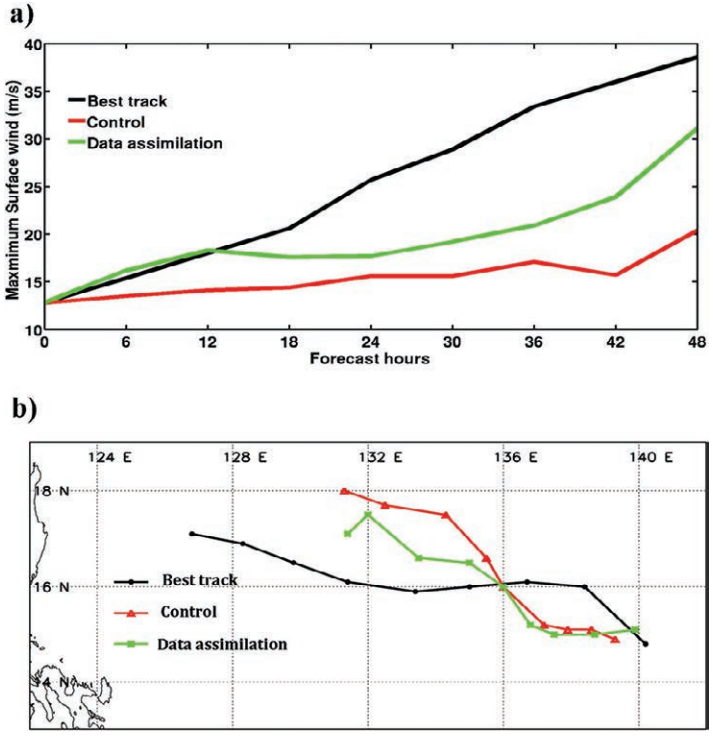

Fig. 10. Impact of actual airborne DWL observations on the numerical simulation of Typhoon Nuri's early rapid intensification. (a) The maximum surface wind and (b) the track from 0000 UTC 17 Aug to 0000 UTC 19 Aug 2008. Forecasts with (green curves) and without (red curves) assimilation of DWL wind are compared with the JTWC best-track data (black curves). DWL data are assimilated for the period 0000–0200 UTC 17 Aug 2008.

At 2000 UTC 16 August 2008, a tropical easterly wave (TCS-013) was located northwest of Guam with a maximum mean wind of about 12.9 m s^{-1}. During the NRL P-3 mission of 16 August, the system was declared tropical depression 13W and was named Tropical Storm Nuri by 18 August 2008. The impact of airborne DWL measurements on the prediction of the formation of Nuri was evaluated by Pu et al. (2010). Results show that the DWL wind data improved the intensity and track forecast for Nuri compared to the assimilation experiment without DWL observations (control). The experiment using DWL data resulted in a more accurate 12–48-h maximum surface wind forecast (Fig. 10a) when compared to the control and verified against the observed surface wind ("best track"), as determined by the Joint Typhoon Warning Center (JTWC), and in a reduction in the northerly bias in the 24–48-h forecast track of Nuri (Fig. 10b). However, the track of Nuri in both the DWL and control experiments was significantly slower than Nuri's observed track. Compared with the control, assimilation of DWL data reduced the error in the 6–48-h surface maximum wind forecast, on average, by 26% and reduced the track forecast error by 18%. DWL data also reduced the error in both the track and intensity forecast for a second case (Typhoon Hagupit; not shown).

The 2008 T-PARC airborne campaign was the first time that DWL measurements were obtained and assimilated during tropical cyclone development. Because no satellite data were assimilated in the experiments with WRF, the impact of the DWL data in these experiments should be viewed as tentative, but, given the sparse DWL data coverage, very encouraging.

Climate change studies. The most comprehensive tool available to analyze climatic trends is the reanalysis technique (Uppala et al. 2005; Simmons et al. 2010). An intercomparison of first-generation reanalyses (Kistler et al. 2001) clearly shows that even such a basic quantity as zonally averaged, time-mean zonal winds are not well constrained by the present observing system. In the tropical upper troposphere and the lower stratosphere, the difference between zonal winds obtained from independent reanalysis efforts are of the same order as the characteristic time variability of this quantity. This does not necessarily imply that the reanalysis technique is inadequate but rather points to the fact that additional wind information is needed to make reanalyses more consistent. Also, more recent reanalysis results show the same features. For example, Fig. 11 shows the zonal wind difference between the most recent reanalysis from ECMWF Re-Analysis (ERA-Interim; see Simmons et al. 2010; Dee et al. 2011) and the second-generation 40-yr ECMWF Re-Analysis (ERA-40; Uppala et al. 2005) for the overlapping time period 1989–2001. The differences are smaller than with Kistler et al. (2001) but the same spatial pattern is found. In addition, as the differences in the stratosphere are emphasized, recent reanalyses have included upper-stratospheric layers. We also find differences in the Arctic and Antarctic regions that are not so apparent in the results from Kistler et al. (2001). The polar area differences are smaller than those found in the tropics, but they point to the need for wind data in the polar atmosphere.

Another aspect of high-latitude wind information is the determination of meridional heat transports. Graversen et al. (2008) have shown that Arctic warming trends in the free troposphere can be, to some extent, explained by an increase in the northward atmospheric heat transport. Graversen et al. (2007) also pointed out that the calculation of meridional heat transports from reanalysis data is restricted by the accuracy of meridional, ageostrophic winds. With the present wind data coverage in the Arctic region, the zonally averaged, meridional wind component is not well constrained. This leads to a spurious mass flux in or out of the Arctic region. Through mass continuity considerations, this mass flux can be adjusted (Trenberth 1997) but improved wind observations are needed to better define the wind field and to make the heat transport calculations more accurate.

Aerosol profiling and pollution transport. Because DWL measurements rely on aerosol backscatter returns to determine line-of-sight velocities, they provide an

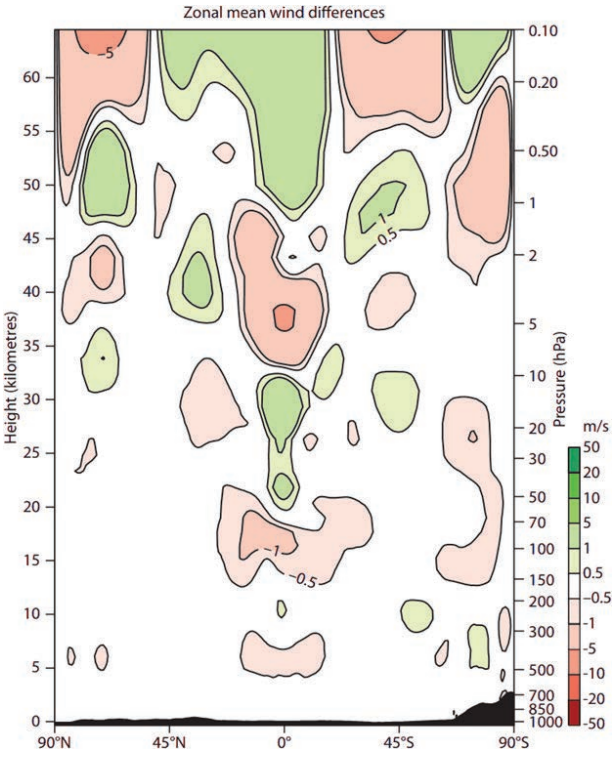

Fig. 11. The zonally averaged latitude–height cross section of zonal mean wind differences (m s^{-1}) between ERA-40 and ERA-Interim for the time period 1989–2001.

excellent opportunity to retrieve profiles of aerosol backscatter and derived aerosol extinction (Ansmann et al. 2007; Flamant et al. 2008). Simultaneous measurements of vertically resolved aerosols and winds are critically needed to address a wide range of air quality and climate change issues associated with long-range pollution transport and aerosol direct and indirect effects. The Cloud–Aerosol Lidar with Orthogonal Polarization (CALIOP) instrument (Winker et al. 2003) on the *Cloud–Aerosol Lidar and Infrared Pathfinder Satellite Observations* (*CALIPSO*) satellite has demonstrated the utility of space-based aerosol backscatter measurements in providing long-term continuous profiling of clouds and aerosols. DWL measurements would extend this record of height-resolved aerosol backscatter measurements and add critical information regarding pollution transport.

Global climate models' predictions of the vertical distribution of aerosols vary widely (Kinne et al. 2006) and, consequently, current model-based estimates of long-range aerosol transport are highly uncertain. Quantifying long-range aerosol transport is critical to address outstanding issues at the nexus of air quality and climate change, particularly in the

Arctic. During Northern Hemisphere late winter and early spring, pollution from Europe, Asia, and North America are transported into the Arctic Basin (Shaw 1995). Because of strong temperature inversions, this pollution accumulates in the Arctic boundary layer, leading to "Arctic haze" (Mitchell 1956). Black carbon is a minor but important component of the Arctic haze (Quinn et al. 2007) and contributes to Arctic warming through direct absorption of solar radiation and can change the surface albedo when it is deposited on the snow and ice (Hansen and Nazarenko 2004). Uncertainties in meridional transport of black carbon into the Arctic are even larger than meridional heat transport due to poor constraints on both wind and aerosols.

TECHNOLOGY USED IN DWL. For over 40 years (Siegman 1966; Huffaker et al. 1970, Benedetti-Michelangeli et al. 1972) ground- and aircraft-based wind lidars have been in development to study atmospheric dynamics, to provide context for pollution transport, and to address uncertainties in the model wind fields. Through recent technology advances that include improved structural materials, higher laser efficiency and output power, and more robust optical coatings, the field of Doppler lidar progressed steadily from the fundamental technology demonstrations of the 1970s and has reached a maturity level needed to make the required wind measurements from space. Please refer to the supplemental material (http://dx.doi.org/10.1175/BAMS-D-12-00164.2) and references listed therein for additional background on wind lidar and the recent studies that have been done on the various types of DWL technologies that are considered for the space-based missions described in the following subsections.

Review of DWL systems. Evolution of lidar technology for space-based measurements has focused on Doppler lidar systems compatible with two primary receiver implementations: coherent detection and direct detection. Early Doppler lidars incorporated coherent detection in the thermal infrared to measure winds based on aerosol backscatter. However, more recent advancements in direct detection technology, which has the advantage of being able to measure winds from atmospheric molecules as well as aerosols, have indicated the feasibility of this technique for space. Coherent and direct detection are briefly discussed below; additional information about the different types of DWL systems may be found in Werner (2004), Henderson et al. (2005), and Reitebuch (2012b). A detailed discussion on the physics of measuring atmospheric wind speed with Doppler lidar is provided in the supplemental material.

CD LIDARS. Coherent detection (CD) lidars use heterodyne detection to estimate the frequency shift between the outgoing and backscattered laser pulses. In these systems, a highly stable but low power local oscillator (LO) laser is first used to seed the outgoing laser pulse. The LO is then optically interfered with the aerosol-backscattered, Doppler-shifted return pulse to produce a temporal beat frequency on the face of the detector. This temporal interference requires that the LO have a long temporal coherence length, so that it does not change frequency during the round-trip time of the emitted and atmospheric-backscattered pulse, and that the wavefront of the return light match that of the LO. The center frequency of the remaining signal corresponds to the positive or negative Doppler shift. CD systems can provide better than 1 m s^{-1} precision on the wind speed estimate in high-aerosol loading conditions or clouds.

Multiple references provide additional information on coherent detection systems (Kavaya et al. 1989, 2014; Henderson et al. 1991; Wagener et al. 1995; among others) and their use in atmospheric boundary layer studies (Post and Cupp 1990; Huffaker and Hardesty 1996; Rothermel et al. 1998; Grund et al. 2001; Banta et al. 2002; Koch et al. 2010; Tucker et al. 2009; Bluestein et al. 2011; de Wekker et al. 2012), wind turbine studies (Käsler et al. 2010), and hazard detection and avoidance at airports (Hannon et al. 2005). Coherent airborne DWLs have also been used to explore the potential impact of future space-based lidars and to develop the necessary advanced signal processing and data interpretation algorithms (Emmitt et al. 2010).

DD LIDARS. In direct detection–spatial interference receivers, a spatial copy of the illumination under spectral investigation is interfered with itself and the frequency estimation is performed on both the outgoing pulse and the atmospheric return. Because the illumination intensity and/or frequency are directly measured without the need for a local oscillator, these systems are referred to as "direct detection" wind lidars. In the direct detection case, the interferometer must remain stable over the round-trip return time. Direct detection (DD) systems include Fabry–Perot etalons used in single-edge (Gentry and Korb 1994), double-edge (Korb et al. 1998; Gentry et al. 2000; ESA 2008; Reitebuch et al. 2009; Dong et al. 2010), or multichannel/fringe-imaging [charge-coupled device (CCD)] configurations (McGill et al. 1997a,b);

fringe-imaging Fizeau (Schillinger et al. 2003; ESA 2008; Reitebuch et al. 2009) and fringe-imaging Michelson (Cézard et al. 2009) interferometers; and Mach–Zehnder interferometers (Liu and Kobayashi 1996; Bruneau 2001; Bruneau and Pelon 2003), including the optical autocovariance receiver, a modified Mach–Zehnder interferometer (Schwiesow and Mayor 1995; Grund and Tucker 2011). Each of these systems can be designed to estimate frequency with narrowband (i.e., aerosol scattered) light or with the wings of the spectrally broadened molecular return or both. The 355-nm double-edge technique discussed in the 2007 NRC decadal survey typically has lower precision (~2–4 m s^{-1}) in the molecular scatter velocity estimates, but it is able to make measurements where aerosol loading is very low. Three different approaches for DD wind measurement are discussed below.

Double-edge detection FP. Edge detection systems typically make use of Fabry–Perot (FP) etalon interferometers to estimate the spectral peak of lidar illumination. FP etalon cavities are designed to transmit light at specific frequencies determined by the spacing of two glass plates (or thickness of a single glass plate), the index of refraction of the medium between the plates, the angle of incidence, and the reflectivity of the optical coatings. For a molecular backscatter double-edge system, two FPs are typically used (i.e., separate etalons, or different spacings on sections of the same etalon). The transmission of each etalon is centered on either side or "edge" of the roughly 600 m s^{-1}-wide molecular backscattered spectrum. The transmission of the atmospheric return through both etalons is detected and compared: an imbalance between the detected signal intensities indicates a positive or negative Doppler shift in the return.

The first molecular "double edge" DWL system was demonstrated by Chanin et al. (1989) and Garnier and Chanin (1992). A double-edge receiver was later built at the Goddard Space Flight Center and installed into the NASA Goddard Lidar Observatory for Wind (GLOW; Gentry et al. 2000) mobile Doppler lidar, which continues to make ground-based wind measurements (Vermeesch et al. 2011). The NASA Tropospheric Wind Lidar Technology Experiment (TWiLITE) instrument, also developed at Goddard, uses a double-edge molecular receiver, operating at the 355-nm wavelength. The TWiLiTE system has been developed for operation aboard NASA's high-altitude ER-2 aircraft as part of a path toward a space-based system. A double-edge FP system comprises the molecular channel of the European Space Agency (ESA)'s Atmospheric Dynamics Mission Aeolus (ADM-Aeolus) instrument (ESA 2008; Reitebuch et al. 2009).

Fringe-imaging systems. In a fringe-imaging configuration, Fabry–Perot etalons may also be used for frequency estimation (McKay 1998). A slightly divergent beam of light incident on a plane-parallel Fabry–Perot produces a circular ring pattern of interference fringes. When properly illuminated, these fringes of equal inclination produce a spatial scan of the spectrum of the incoming light where the wavelength is proportional to the radial distance from the center of the ring pattern. The ring pattern may then be imaged on a CCD or focal plane array or modified via special optical components to produce either lines or rings (Hays 1990; Dehring et al. 2005; Irgang et al. 2002) or points (McGill et al. 1997c). The difference between the outgoing pulse fringe pattern and the atmospheric return pattern relates to the Doppler shift/wind measurement. A similar fringe-imaging design using a Mach–Zehnder interferometer has also been investigated (Bruneau 2002). A fringe-imaging Fizeau interferometer system (Schillinger et al. 2003; Reitebuch et al. 2009) is currently being integrated into the aerosol channel of the European ADM-Aeolus mission instrument.

Optical autocovariance. In recent years, Ball Aerospace and Technologies Corporation has developed another type of wind lidar receiver using optical autocovariance techniques (Schwiesow and Mayor 1995). The resulting Optical Autocovariance Wind Lidar (OAWL) is a modified Mach–Zehnder interferometer (Liu and Kobayashi 1996) that uses cat's eye mirrors to increase the interferometer's field of view (Grund and Tucker 2011). The OAWL estimates line-of-sight wind speeds by measuring the Doppler shifts in atmospheric aerosol returns at the 355- and/or 532-nm wavelengths. The OAWL design may be shifted to operate at any wavelength (Grund et al. 2009), or paired with a molecular return channel (i.e., double-edge Fabry–Perot) system operating at 355 nm. The resulting full direct detection system would require only one 355-nm laser to make measurements from both the molecular and aerosol returns in the atmosphere.

Technical readiness and advancements in space-based lidar. Underlying the different design concepts discussed in the following subsections, the level of technical readiness remains one of the most important factors in preparing a wind lidar mission for space. One of the greatest challenges for space-based lidar

is building and space qualifying the pulsed laser capable of providing the power, stability, and lifetime required. Specific requirements on the laser including wavelength, power, pulse bandwidth, pulse repetition frequency, and frequency stability depend on the type of system and are driven by performance guidance, an example of which is given in Table ES1 (http://dx.doi.org/10.1175/BAMS-D-12-00164.2).

All DWL systems require a single-longitudinal-mode (single wavelength) laser and all must address challenges in laser lifetime, prevention of laser optical damage, and laser electrical efficiency. Significant effort has been made internationally to space readiness for high-power lasers at the Nd:YAG crystal wavelengths of 1 mm doubled to 532 nm and tripled to 355 nm. These wavelengths apply not only to wind lidar but also to systems such as the laser on NASA's Ice, Cloud, and Land Elevation Satellite-2 (ICESat-2) mission (Sawruk et al. 2013). Likewise, systems using these wavelengths benefit from the experience in laser qualification and laser lifetime gained from the CALIOP system on the *CALIPSO* payload (Weimer et al. 2004; Hovis 2006; Hunt et al. 2009), which, as of this writing, has been operating continuously for over 7 years.

Significant investment has also been made in developing high-power 2-μm wavelength coherent detection systems. Since the mid-1990s NASA's Langley Research Center (LaRC) has worked toward development of a space-based coherent detection lidar, including a 2-μm detector development and a laser development program that has produced a laser with greater than 1-J pulse energies at 10 Hz (Kavaya et al. 2014).

In addition to laser qualification for space, several figures of merit are very important for space missions: reliability, electrical efficiency, cooling requirements, mass, and electrical power needs. NASA tracks the development of technology for space missions using technical readiness levels (TRLs; Mankins 1995), which help to focus risk reduction efforts for future missions. As part of the development of DWL systems for space, airborne demonstrations help to increase a system's TRL by demonstrating operation from a high-altitude platform. The Doppler Aerosol Wind Lidar (DAWN; Braun et al. 2013; Kavaya et al. 2014), TWiLiTE (Gentry et al. 2011), OAWL (Tucker et al. 2012), and ADM-Aeolus airborne demonstrator (Paffrath et al. 2009; Reitebuch et al. 2009) systems have all flown in aircraft, helping to raise the TRLs of the various technologies. These airborne systems may also provide ground- or aircraft-based validation data after a DWL system has been launched.

Profiling wind through the troposphere and lower stratosphere: Full DD and hybrid system concepts. The lidar technologies discussed in the previous section take advantage of laser light backscattered from molecules present throughout the atmospheric column or from aerosols, which are present mainly in the lower troposphere or as thin cirrus at higher altitudes. Some systems operating at high (i.e., ultraviolet) frequencies can take advantage of both aerosol and molecular lidar return. Recent design concepts for space-based wind lidars employ separate receivers to measure Doppler shifts from the aerosols and molecules. In the full direct detection systems, the aerosol and molecular receivers share the same laser and telescope. In the so-called hybrid systems, the two receivers operate at two different laser frequencies but share the same telescope(s). The following subsections describe some recently studied or implemented instrument concepts for measuring atmospheric winds: the ADM-Aeolus system (ESA 2008; LeRille et al. 2012; Reitebuch 2012a), the hybrid system for the U.S. GWOS, and systems for a Winds from the International Space Station for Climate Research (WISSCR) mission.

THE ESA ADM-AEOLUS SINGLE-WAVELENGTH FULL DIRECT DETECTION SYSTEM. The first spaceborne demonstration of DWL technology will be provided by the ESA's ADM-Aeolus (Stoffelen et al. 2005). ADM-Aeolus features a single 355-nm laser transmitter and two direct detection systems: a double-edge FP etalon for the molecular return and a fringe-imaging Fizeau spectrometer for the aerosol returns (Endemann 2006; LeRille et al. 2012). Subsequent to the 2005 report, several technical modifications have been made to the Aeolus instrument, the most important being changing from burst to continuous operations. The instrument development and expected science capabilities are well documented and highlighted in a special issue of *Tellus A* (2007, Vol. 60, No. 2). Likewise, ESA (2008) discusses the mission objectives, scientific impact studies, and technology, and LeRille et al. (2012) and Reitebuch (2012a) provide the most recent status of ADM-Aeolus.

ADM-Aeolus presently has a planned launch date in 2015 and the expected mission lifetime is 3 years. Line-of-sight (LOS) wind profiles from ADM-Aeolus are expected to give a significant positive impact on NWP analysis quality—in particular, in the tropics at upper levels, where only a limited amount of high-quality wind data is available in the current observing system. Several studies have demonstrated the potential impact of the ADM-Aeolus instrument on NWP forecast quality. Cress and Wergen

(2001) demonstrated the significant impact from withholding existing wind profile information over the North American continent on European forecast quality. Žagar et al. (2004) emphasized the potential impact in the tropics and showed how single line-of-sight wind measurements and mass information can complement each other. As ADM-Aeolus will only measure a single-component wind profile, the full wind information can only be retrieved in a data assimilation system where other observational information is used to complement the ADM-Aeolus winds. Tan et al. (2007) demonstrated the impact of ADM-Aeolus-type wind information on ensemble assimilation systems, while Marseille et al. (2007) and Stoffelen et al. (2006) discussed the ADM-Aeolus impact on OSSE type of experiments. All these studies show that ADM-Aeolus will have a significant impact on NWP quality if the wind observations fulfill the accuracy requirements. Recent experiments confirm that these impact results also hold for the continuous-mode instrument. Furthermore, the ADM-Aeolus instrument can also give information on aerosol concentrations in the atmosphere as discussed by Ansmann et al. (2007) and Flamant et al. (2008).

Studies have been conducted to develop user requirements for an Aeolus follow-on mission. From these studies in the extratropics, wind component profile coverage appears adequate in lieu of obtaining two independent measurement perspectives, while in the tropics both zonal and meridional wind profiles are important. A complement of a side- and back-looking Aeolus-type instrument would fulfill the stated requirements (Stoffelen et al. 2008). If ADM-Aeolus successfully demonstrates the feasibility and utility of space-based Doppler wind lidars, then the period 2016–18 may be unique among the atmospheric data records in providing global wind data coverage and therefore better atmospheric analysis accuracy. Follow-on missions have been considered but future planning awaits the successful demonstration of ADM-Aeolus wind-measuring capabilities. In this respect, ESA's ADM-Aeolus is leading in demonstrating that a DWL can fulfill user requirements on wind profiling and is expected to deliver a well-characterized satellite instrument concept that could be the baseline for follow-on missions.

THE NASA GWOS HYBRID CONCEPT. The GWOS, a mission concept proposed to the NRC decadal survey (NRC 2007), was designed for a winds demonstration mission from a free-flyer satellite in LEO orbit. In addition to component technology advances, important differences from the system concept discussed in Baker et al. (1995) were inclusion of both direct and coherent detection lidar subsystems in a hybrid configuration, and an improved methodology for achieving multiple look angles through telescopes that are shared between the two lidar subsystems. The hybrid concept includes a coherent detection system at the 2-μm wavelength for aerosol return and a double-edge direct detection at the 355-nm wavelength for molecular return. In the GWOS design, scanning is achieved by switching between four fixed conventional telescopes, thus reducing technology risk, angular momentum transients, and power that would be required for scanning a full telescope. Marx et al. (2010) at NASA GSFC have recently completed the build and test of a prototype for the GWOS four-look telescope system. Figure 12 shows the geometry for the GWOS mission concept as an example for an orbiting spacecraft with a DWL; a detailed explanation may be found in the supplemental material, and Fig. 13 illustrates the nominal 24-h GWOS data coverage from sun-synchronous orbit.

THE WISSCR CONCEPTS. In late 2010/early 2011, an Instrument Design Laboratory (IDL)/Mission Design

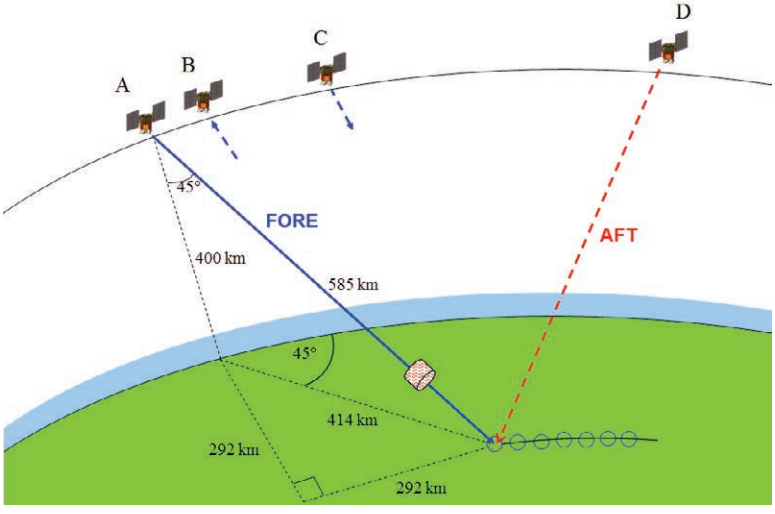

FIG. 12. The orbital geometry for the GWOS mission concept. Points A–D are defined as follows: A is the first forward +45°-azimuth laser shot fired into the atmospheric sample volume; B is the backscattered light from the first shot received from Earth's surface and the conclusion of the atmospheric return from the first shot; C is the second forward +45°-azimuth laser shot fired; and D is the first aft +135°-azimuth laser shot fired into the same atmospheric sample volume about 81 s after position A. Not drawn to scale.

Laboratory (MDL) study was conducted at GSFC to determine the feasibility of using the International Space Station for a DWL mission referred to as the WISSCR concept (Emmitt et al. 2011b). This study and a subsequent WISSCR-like study conducted in 2012 to investigate the feasibility of deploying OAWL on the International Space Station (ISS) are described in the supplemental material.

Comparison of three DWL space-based approaches. Table 1 compares some attributes of the ADM-Aeolus system concept with the GWOS and WISSCR concepts. As a demonstration mission, ADM-Aeolus has a single-perspective view of the target volume and only measures winds along a single line-of-sight from the satellite, whereas GWOS and WISSCR would provide two perspectives into the measurement volume. Horizontal resolution in the table refers to along-track spacing between observations. ADM-Aeolus and WISSCR make measurements along a single track, whereas GWOS makes measurements along two tracks, one on each side of the orbital track. Because ADM-Aeolus will be deployed in sun-synchronous orbit, important science questions can be addressed for both the tropics and the polar regions.

CONCLUDING REMARKS. In recent years, our understanding of the important role that a space-based DWL would have in the global observing system has reached the point where we are confident major advances would result in both NWP applications and climate change research. ESA's ADM-Aeolus DWL, with its single line-of-sight wind measurements, now scheduled for launch in 2015, will be a significant step forward. The two-perspective DWL concepts currently being investigated will build on the initial ESA deployment. Opportunities such as NASA's Earth Venture class of missions in the Earth System Science Pathfinder program (see

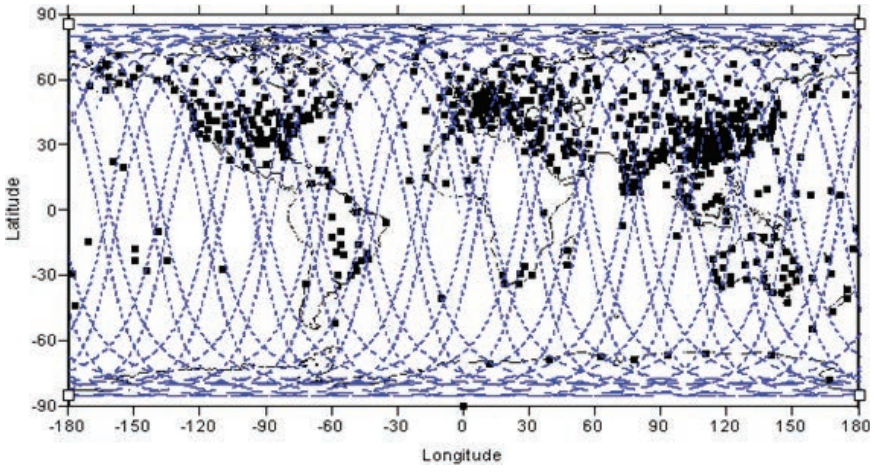

Fig. 13. The 24-h measurement coverage for GWOS, along with the locations of radiosondes collected during a 24-h period. There are two parallel data tracks for GWOS, provided by its four fixed telescopes, with a pair of fore and aft telescopes viewing the atmospheric measurement volume on each side of the spacecraft. Data coverage would be the same for ADM, but with a single data track and a single perspective. Similarly for WIISCR, there would be one data track (with both fore and aft perspectives) but within ±54° of latitude, given the 51.6° ISS orbit.

Table 1. Comparison of some key attributes for ADM-Aeolus, GWOS, and WISSCR.

Attribute	ADM-Aeolus	GWOS	WISSCR
Orbit altitude (km)	400	400	350–400
Orbit inclination	98° sun-synchronous	98° sun-synchronous	51.6°
Number of LOS	1	4	2
Profiles per orbit	~460 single-component profiles	~229 horizontal vectors	~110 vectors (low resolution) ~880 vectors (high resolution)
Horizontal resolution	~100 km between single-component profiles on one side of ground track	350 km with full profile on both sides of ground track	Variable (~30–350 km) with full profiles on one side of ground track
Vertical resolution (km)	PBL: 0.25–0.5 Troposphere: 1 Stratosphere: 2	PBL: 0.25–0.5 Troposphere: 1–2 Stratosphere: 2	PBL: 0.25–0.5 Troposphere: 1–2 Stratosphere: 2

http://science.nasa.gov/about-us/smd-programs/earth-system-science-pathfinder/) are being pursued with the goal of deploying a U.S. space-based DWL as soon as possible.

ACKNOWLEDGMENTS. The authors thank Dr. Ramesh Kakar of the Earth Science Division at NASA headquarters and Dr. George Komar of the NASA Earth Science Technology Office at the Goddard Space Flight Center for supporting research with DWL data, including airborne campaigns, and funding hardware risk reduction studies to advance the readiness of the DWL technology for space. The authors thank Dr. John Cortinas and NOAA's Office of Weather and Air Quality for contributing to the support for DWL OSSEs through NOAA's OSSE Testbed. The expert assistance of Paul Berrisford of ECMWF is sincerely acknowledged. Sidney Wood and Steven Greco of Simpson Weather Associates (SWA) are acknowledged for their dedication to producing simulated space-based DWL observations used in the OSSEs and processing and analyzing data from the U.S. Navy's airborne DWL. Funding for manuscript preparation and submission was provided by SWA. M. Weissmann is part of the Hans-Ertel Centre for Weather Research, a network of universities, research institutes, and Deutscher Wetterdienst funded by the German Federal Ministry of Transport, Building and Urban Development.

The manuscript was significantly improved by addressing the comments of three anonymous reviewers. Prof. Richard Somerville and Dr. Ross Hoffman also provided valuable comments.

REFERENCES

Andersson, E., and M. Masutani, 2010: Collaboration on observing system simulation experiments (Joint OSSE). *ECMWF Newsletter,* No. 123, ECMWF, Reading, United Kingdom, 14–16.

Ansmann, A., U. Wandinger, O. Le Rille, D. Lajas, and A. G. Straume, 2007: Particle backscatter and extinction profiling with the spaceborne high-spectral-resolution Doppler lidar ALADIN: Methodology and simulations. *Appl. Opt.,* **46,** 6606–6622, doi:10.1364/AO.46.006606.

Anthes, R. A., and Coauthors, 2008: The COSMIC/FORMOSAT-3 mission: Early results. *Bull. Amer. Meteor. Soc.,* **89,** 313–333.

Atlas, R., 1997: Atmospheric observations and experiments to assess their usefulness in data assimilation. *J. Meteor. Soc. Japan,* **75,** 111–130.

——, and G. D. Emmitt, 2008: Review of observing system simulation experiments to evaluate the potential impact of lidar winds. *24th International Laser Radar Conference 2008 (ILRC24),* Vol. 2, Curran Associates, 726–729.

——, and L. P. Riishojgaard, 2008: Application of OSSEs to observing system design. *Remote Sensing System Engineering,* P. E. Ardanuy and J. J. Puschell, Eds., International Society for Optical Engineering (SPIE Proceedings, Vol. 7087), 708707, doi:10.1117/12.795344.

——, E. Kalnay, W. E. Baker, J. Susskind, D. Reuter, and M. Halem, 1985a: Simulation studies of the impact of future observing systems on weather prediction. Preprints, *Seventh Conf. on Numerical Weather Prediction,* Montreal, QC, Canada, Amer. Meteor. Soc., 145–151.

——, ——, and M. Halem, 1985b: Impact of satellite temperature sounding and wind data on numerical weather prediction. *Opt. Eng.,* **24,** 341–346.

——, A. Y. Hou, and O. Reale, 2005a: Application of SeaWinds scatterometer and TMI-SSM/I rain rates to hurricane analysis and forecasting. *J. Photogramm. Remote Sens.,* **59,** 233–243.

——, and Coauthors, 2005b: Hurricane forecasting with the high-resolution NASA finite volume general circulation model. *Geophys. Res. Lett.,* **32,** L03807, doi:10.1029/2004GL021513.

Baker, N. L., 2000: Observation adjoint sensitivity and the adaptive observation-targeting problem. Ph.D. dissertation, Naval Postgraduate School, 265 pp.

——, and R. H. Langland, 2008: Diagnostics for evaluating the impact of satellite observations. Recent developments in the use of satellite observations in numerical weather prediction, ECMWF Seminar Proceedings, 309–326.

——, and ——, 2009: Diagnostics for evaluating the impact of satellite observations. *Data Assimilation for Atmospheric, Oceanic and Hydrologic Applications,* S. K. Park and L. Xu, Eds., Springer, 177–196.

Baker, W. E., and Coauthors, 1995: Lidar-measured winds from space: A key component for weather and climate prediction. *Bull. Amer. Meteor. Soc.,* **76,** 869–888.

Banta, R. M., R. K. Newsom, J. K. Lundquist, Y. L. Pichugina, R. L. Coulter, and L. Mahrt, 2002: Nocturnal low-level jet characteristics over Kansas during CASES-99. *Bound.-Layer Meteor.,* **105,** 221–252.

Barker, D. M., W. Huang, Y.-R. Guo, A. J. Bourgeois, and Q. N. Xiao, 2004: A three-dimensional variational data assimilation system for MM5: Implementation and initial results. *Mon. Wea. Rev.,* **132,** 897–914.

Benedetti-Michelangeli, G., F. Congeduti, and G. Fiocco, 1972: Measurement of aerosol motion and wind velocity in the lower troposhere by Doppler optical radar. *J. Atmos. Sci.,* **29,** 906–910.

Bluestein, H. B., G. D. Emmitt, J. Houser, and R. Bluth, 2011: On the use of a mobile Doppler lidar to probe the boundary layer near and in tornadic and non-tornadic supercells. Preprints, *Fifth Symp. on Lidar Atmospheric Applications,* Seattle, WA, Amer. Meteor. Soc., 6.5. [Available online at https://ams.confex.com/ams/91Annual/webprogram/Paper179772.html.]

Braun, S., and Coauthors, 2013: NASA's Genesis and Rapid Intensification Processes (GRIP) Field Experiment. *Bull. Amer. Meteor. Soc.,* **94,** 345–363.

Bruneau, B., and J. Pelon, 2003: Simultaneous measurements of particle backscattering and extinction coefficients and wind velocity by lidar with a Mach-Zehnder interferometer: Principle of operation and performance assessment. *Appl. Opt.,* **42,** 1101–1114.

Bruneau, D., 2001: Mach-Zehnder interferometer as a spectral analyzer for molecular Doppler wind lidar. *Appl. Opt.,* **40,** 391–399.

——, 2002: Fringe-imaging Mach-Zehnder interferometer as a spectral analyzer for molecular Doppler wind lidar. *Appl. Opt.,* **41,** 503–510.

Cardinali, C., 2009: Monitoring the observation impact on the short-range forecast. *Quart. J. Roy. Meteor. Soc.,* **135,** 239–250.

——, S. Pezzulli, and E. Andersson, 2004: Influence-matrix diagnostic of a data assimilation system. *Quart. J. Roy. Meteor. Soc.,* **130,** 2767–2786.

Cézard, N., A. Dolfi-Bouteyre, J.-P. Huignard, and P. H. Flamant, 2009: Performance evaluation of a dual fringe-imaging Michelson interferometer for air parameter measurements with a 355 nm Rayleigh-Mie lidar. *Appl. Opt.,* **48,** 2321–2332.

Chanin, M. L., A. Garnier, A. Hauchecorn, and J. Porteneuve, 1989: A Doppler lidar for measuring winds in the middle atmosphere. *Geophys. Res. Lett.,* **16,** 1273–1276.

Chen, J. Y., B. E. Carlson, and A. D. Del Genio, 2002: Evidence for strengthening of the tropical general circulation in the 1990s. *Science,* **295,** 838–841.

Cress, A., and W. Wergen, 2001: Impact of profile observations on the German Weather Service's NWP system. *Meteor. Z.,* **10,** 91–101.

Dee, D. P., and S. Uppala, 2009: Variational bias correction of satellite radiance data in the ERA-Interim reanalysis. *Quart. J. Roy. Meteor. Soc.,* **135,** 1830–1841.

——, and Coauthors, 2011: The ERA-Interim reanalysis: Configuration and performance of the data assimilation system. *Quart. J. Roy. Meteor. Soc.,* **137,** 553–597.

Dehring, M. T., J. M. Ryan, P. B. Hays, B. Moore III, and J. Wang, 2005: GroundWinds balloon fringe-imaging Doppler lidar mission concept and instrument performance. *Lidar Remote Sensing for Industry and Environmental Monitoring V,* U. N. Singh and K. Mizutani, Eds., International Society for Optical Engineering (SPIE Proceedings, Vol. 5653), doi:10.1117/12.580170.

de Wekker, S. F. J., K. S. Godwin, G. D. Emmitt, and S. Greco, 2012: Airborne Doppler lidar measurements of valley flows in complex coastal terrain. *J. Appl. Meteor. Climatol.,* **51,** 1558–1574.

Dong, J., and Coauthors, 2010: Doppler lidar measurement of wind in the stratosphere. *J. Opt. Soc. Korea,* **14,** 199–203.

Emmitt, G. D., S. Greco, and S. Wood, 2010: Using an airborne Doppler wind lidar to explore the potential impact of a future space-based wind lidar, particularly in the case of tropical cyclones. Preprints, *14th Symp. on Integrated Observing and Assimilation Systems for the Atmosphere, Oceans, and Land Surface (IOAS-AOLS),* Atlanta, GA, Amer. Meteor. Soc., 1.3. [Available online at https://ams.confex.com/ams/90annual/techprogram/paper_165444.htm.]

——, Z. Pu, K. Godwin, and S. Greco, 2011a: Airborne Doppler wind lidar data impacts on tropical cyclone track and intensity forecasting: The data processing, interpretation and assimilation. Preprints, *15th Symp. on Integrated Observing and Assimilation Systems for the Atmosphere, Oceans and Land Surface (IOAS-AOLS),* Seattle, WA, Amer. Meteor. Soc., 9.2. [Available online at https://ams.confex.com/ams/91Annual/webprogram/Paper182343.html.]

——, S. A. Wood, M. J. Kavaya, B. Gentry, and W. Baker, 2011b: Technology and data utility challenges for a Doppler wind lidar on the International Space Station. Preprints, *15th Symp. on Integrated Observing and Assimilation Systems for the Atmosphere, Oceans, and Land Surface (IOAS-AOLS),* Seattle, WA, Amer. Meteor. Soc., 2.2. [Available online at https://ams.confex.com/ams/91Annual/webprogram/Paper182281.html.]

Endemann, M., 2006: ADM-Aeolus: The first spaceborne wind lidar. *Lidar Remote Sensing for Environmental Monitoring VII,* U. N. Singh, T. Itabe, and D. Narayana Rao, Eds., International Society for Optical Engineering (SPIE Proceedings, Vol. 6409), 64090G, doi:10.1117/12.697081.

ESA, 2008: ADM-Aeolus science report. P. Clissold, Ed., European Space Agency Rep. ESA SP-1311, 121 pp.

Flamant, P. H., J. Cuesta, M.-L. Denneulin, A. Dabas, and D. Huber, 2008: ADM-Aeolus retrieval algorithms for aerosol and cloud products. *Tellus,* **60A,** 273–286, doi:10.1111/j.1600-0870.2007.00287.x.

Garnier, A., and M. L. Chanin, 1992: Description of a Doppler Rayleigh lidar for measuring winds in the middle atmosphere. *Appl. Phys.*, **55B,** 35–40.

Gelaro, R., R. H. Langland, S. Pellerin, and R. Todling, 2010: The THORPEX observation impact intercomparison experiment. *Mon. Wea. Rev.,* **138,** 4009–4025.

Gentry, B. M., and C. L. Korb, 1994: Edge technique for high-accuracy Doppler velocimetry. *Appl. Opt.,* **33,** 5770–5777.

——, H. Chen, and S. X. Li, 2000: Wind measurements with 355-nm molecular Doppler lidar. *Opt. Lett.,* **25,** 1231–1233.

——, ——, J. Cervantes, R. Machan, D. Reed, R. Cargo, C. Marx, and P. Jordan, 2011: Airborne testing of the TWiLiTE direct detection Doppler lidar. *16th Coherent Laser Radar Conference 2011 (CLRC XVI),* Curran Associates, 164–167.

Graversen, R. G., 2006: Do changes in the midlatitude circulation have any impact on the Arctic surface temperature trend? *J. Climate,* **19,** 5422–5438.

——, E. Källén, M. Tjernström, and H. Körnich, 2007: Atmospheric mass-transport inconsistencies in the ERA-40 reanalysis. *Quart. J. Roy. Meteor. Soc.,* **133,** 673–680.

——, T. Mauritsen, M. Tjernström, E. Källén, and G. Svensson, 2008: Vertical structure of recent Arctic warming. *Nature,* **451,** 53–56.

Grund, C. J., and S. C. Tucker, 2011: Optical Autocovariance Wind Lidar (OAWL): A new approach to direct-detection Doppler wind profiling. Preprints, *Fifth Symp. on Lidar,* Seattle, WA, Amer. Meteor. Soc., 4.9. [Available online at https://ams.confex.com/ams/91Annual/webprogram/Paper188184.html.]

——, R. M. Banta, J. L. George, J. N. Howell, M. J. Post, R. A. Richter, and A. M. Weickmann, 2001: High-resolution Doppler lidar for boundary layer and cloud research. *J. Atmos. Oceanic Technol.,* **18,** 376–393.

——, J. Howell, R. Pierce, M. Stephens, 2009: Optical autocovariance direct detection lidar for simultaneous wind, aerosol, and chemistry profiling from ground, air, and space platforms. *Advanced Environmental, Chemical, and Biological Sensing Technologies VI.* T. Vo-Dinh, R. A. Lieberman, and G. Gauglitz, Eds., International Society for Optical Engineering (SPIE Proceedings, Vol. 7312), doi:10.1117/12.824204.

Hannon, S. M., K. S. Barr, D. K. Jacob, and M. W. Phillips, 2005: Application of pulsed Doppler lidar in the airport terminal area. *Lidar Remote Sensing for Industry and Environmental Monitoring V,* S. M. Hannon et al., Eds., International Society for Optical Engineering (SPIE Proceedings Vol. 5653), doi:10.1117/12.579037.

Hansen, J., and L. Nazarenko, 2004: Soot climate forcing via snow and ice albedos. *Proc. Natl. Acad. Sci. USA,* **101,** 423–428, doi:10.1073/pnas.2237157100.

Hays, P. B., 1990: Circle to line interferometer optical system. *Appl. Opt.,* **29,** 1482–1489.

Henderson, S. W., P. Gatt, D. Rees, and R. M. Huffaker, 2005: Wind lidar. *Laser Remote Sensing,* T. Fujii and T. Fukuchi, Eds., Optical Science and Engineering Series, Vol. 97, CRC Press, 469–722.

Houchi, K., A. Stoffelen, G. J. Marseille, and J. de Kloe, 2010: Comparison of wind and wind shear climatologies derived from high-resolution radiosondes and the ECMWF model. *J. Geophys. Res.,* **115,** D22123, doi:10.1029/2009JD013196.

Hovis, F. E., 2006: Qualification of the laser transmitter for the CALIPSO aerosol lidar mission. *Solid State Lasers XV: Technology and Devices,* H. J. Hoffman and R. K. Shori, Eds., International Society for Optical Engineering (SPIE Proceedings, Vol. 6100), 61001X, doi:10.1117/12.659748.

Huffaker, R. M., and R. M. Hardesty, 1996: Remote sensing of atmospheric wind velocities using solid-state and CO_2 coherent laser systems. *Proc. IEEE,* **84,** 181–204.

——, A. V. Jelalian, and J. A. L. Thomson, 1970: Laser-Doppler system for detection of aircraft trailing vortices. *Proc. IEEE,* **58,** 322–326.

Hunt, W. H., D. M. Winker, M. A. Vaughan, K. A. Powell, P. L. Lucker, and C. Weimer, 2009: *CALIPSO* lidar description and performance assessment. *J. Atmos. Oceanic Technol.,* **26,** 1214–1228.

Irgang, T. D., P. B. Hays, and W. R. Skinner, 2002: Two-channel direct-detection Doppler lidar employing a charge-coupled device as a detector. *Appl. Opt.*, **41**, 1145–1155.

Källén, E., D. Tan, C. Cardinali, and P. Berrisford, 2010: Spaceborne Doppler wind lidars – Scientific Motivation and Impact Studies for ADM/Aeolus. *33rd Meeting of the Working Group on Space-Based Lidar Winds,* Destin, FL, CIRES. [Available online at http://cires.colorado.edu/events/lidarworkshop/LWG/Feb10/Papers.feb10/Kallen.feb10.ppt.]

Käsler, Y., S. Rahm, R. Simmet, and M. Kühn, 2010: Wake measurements of a multi-MW wind turbine with coherent long-range pulsed Doppler wind lidar. *J. Atmos. Oceanic Technol.,* **27,** 1529–1532.

Kavaya, M. J., S. W. Henderson, J. R. Magee, C. P. Hale, and R. M. Huffaker, 1989: Remote wind profiling with a solid-state Nd:YAG coherent lidar system. *Opt. Lett.,* **14,** 776–778.

——, J. Y. Beyon, G. J. Koch, M. Petros, P. J. Petzar, U. N. Singh, B. C. Trieu, and J. Yu, 2014: The Doppler Aerosol Wind Lidar (DAWN) airborne, wind-profiling, coherent-detection lidar system: Overview and preliminary flight results. *J. Atmos. Oceanic Technol.,* in press.

Key, J., D. Santek, C. S. Velden, N. Bormann, J.-N. Thepaut, L. P. Riishojgaard, Y. Zhu, and W. P. Menzel, 2003: Cloud-drift and water vapor winds in the polar regions from MODIS. *IEEE Trans. Geosci. Remote Sens.,* **41,** 482–492.

Kinne, S., and Coauthors., 2006: An AeroCom initial assessment—Optical properties in aerosol component modules of global models. *Atmos. Chem. Phys.*, **6**, 1815–1834.

Kistler, R., and Coauthors, 2001: The NCEP–NCAR 50–Year Reanalysis: Monthly means CD–ROM and documentation. *Bull. Amer. Meteor. Soc.,* **82,** 247–267.

Kleist, D. T., D. F. Parrish, J. C. Derber, R. Treadon, W.-S. Wu, and S. Lord, 2009: Introduction of the GSI into the NCEP Global Data Assimilation System. *Wea. Forecasting,* **24,** 1691–1705.

Korb, C. L., B. M. Gentry, S. X. Li, and C., 1998: Theory of the double-edge technique for Doppler lidar wind measurement. *Appl. Opt.,* **37,** 3097–3104.

Langland, R. H., and N. L. Baker, 2004: Estimation of observation impact using the NRL atmospheric variational data assimilation adjoint system. *Tellus,* **56A,** 189–201.

——, and R. N. Maue, 2012: Uncertainty in operational atmospheric analyses. *Proc. Fifth WMO Workshop on the Impact of Various Observing Systems on Numerical Weather Prediction,* Sedona, AZ, WMO. [Available online at www.wmo.int/pages/prog/www/OSY/Meetings/NWP5_Sedona2012/1a1_Langland.pdf.]

——, ——, and C. H. Bishop, 2008: Uncertainty in atmospheric temperature analyses. *Tellus,* **60A,** 598–603.

LeRille, O., M. Endemann, A. Culoma, and D. Wernham, 2012: ADM-Aeolus: ESA's high spectral resolution Doppler wind lidar mission: Recent achievements and future prospects. *Proc. 26th Int. Laser Radar Conf.,* Porto Heli, Greece, NASA, S4O-01.

Liu, Z., and T. Kobayashi, 1996: Differential discrimination technique for incoherent Doppler lidar to measure atmospheric wind and backscatter ratio. *Opt. Rev.,* **3,** 47–52.

Mankins, J. C., 1995: Technology readiness levels—A white paper. NASA, 5 pp. [Available online at www.hq.nasa.gov/office/codeq/trl/trl.pdf.]

Marseille, G.-J., A. Stoffelen, and J. Barkmeijer, 2007: Impact assessment of prospective spaceborne Doppler wind lidar observation scenarios. *Tellus,* **60A,** 234–248.

——, ——, and ——, 2008: A cycled sensitivity observing system experiment on simulated Doppler wind lidar data during the 1999 Christmas storm "Martin." *Tellus,* **60A,** 249–260, doi:10.1111/j.1600-0870.2007.00290.x.

Marx, C., B. Gentry, M. Kavaya, P. Jordan, and E. Faust, 2010: Hybrid Doppler Wind Lidar (HDWL) transceiver ACT project. *33rd Meeting of the Working Group on Space-Based Lidar Winds,* Destin, FL, CIRES. [Available online at http://cires.colorado.edu/events/lidarworkshop/LWG/Feb10/Papers.feb10/Marx.feb10.pdf.]

Masutani, M., and Coauthors, 2010: Observing system simulation experiments at the National Centers for Environmental Prediction. *J. Geophys. Res.,* **115,** D07101, doi:10.1029/2009JD012528.

McGill, M. J., W. R. Skinner, and T. D. Irgang, 1997a: Analysis techniques for the recovery of winds and backscatter coefficients from a multiple-channel incoherent Doppler lidar. *Appl. Opt.,* **36,** 1253–1268.

——, ——, and ——, 1997b: Validation of wind profiles measured with incoherent Doppler lidar. *Appl. Opt.,* **36,** 1928–1932.

——, M. Marzouk, V. S. Scott III, and J. D. Spinhirne, 1997c: Holographic circle-to-point converter with particular applications for lidar work. *Opt. Eng.,* **36,** 2171–2175, doi:10.1117/1.601437.

McKay, J. A., 1998: Modeling of direct detection Doppler wind lidar. II. The fringe imaging technique. *Appl. Opt.,* **37,** 6487–6493.

Mitas, C. M., and A. Clement, 2005: Has the Hadley cell been strengthening in recent decades? *Geophys. Res. Lett.,* **32,** L03809, doi:10.1029/2004GL021765.

——, and ——, 2006: Recent behavior of the Hadley cell and tropical thermodynamics in climate models and reanalyses. *Geophys. Res. Lett.,* **33,** L01810, doi:10.1029/2005GL024406.

Mitchell, J. M., 1956: Visual range in the polar regions with particular reference to the Alaskan Arctic. *J. Atmos. Terr. Phys.,* **1** (Suppl.), 195–211.

Miyakoda, K., R. D. Hembree, R. F. Strickler, and I. Shulman, 1972: Cumulative results of extended forecast experiments. I. Model performance for winter cases. *Mon. Wea. Rev.,* **100,** 836–855.

NRC, 2007: *Earth Science and Applications from Space: National Imperatives for the Next Decade and Beyond.* The National Academies Press, 456 pp.

Ota, Y., J. C. Derber, E. Kalnay, and T. Miyoshi, 2013: Ensemble-based observation impact estimates using the NCEP GFS. *Tellus,* **65A,** 20038, doi:10.3402/tellusa.v65i0.20038.

Paffrath, U., C. Lemmerz, O. Reitebuch, B. Witschas, I. Nikolaus, and V. Freudenthaler, 2009: The airborne demonstrator for the direct-detection Doppler wind lidar ALADIN on ADM-Aeolus. Part II: Simulations and Rayleigh receiver radiometric performance. *J. Atmos. Oceanic Technol.,* **26,** 2516–2530.

Petzar, P., and Coauthors, 2010: Field testing of a high-energy 2-mm Doppler lidar. *J. Appl. Remote Sens.,* **4,** 043512, doi:10.1117/1.3368726.

Post, M. J., and R. E. Cupp, 1990: Optimizing a pulsed Doppler lidar. *Appl. Opt.,* **29,** 4145–4158.

Pu, Z., B. Gentry, and B. B. Demoz, 2009: Potential impact of lidar wind measurements on high-impact weather forecasting: A regional OSSEs study. Preprints, *13th Conf. on Integrated Observing Systems for Atmosphere, Ocean, and Land Surface (IOAS-AOLS),* Phoenix, AZ, Amer. Meteor. Soc., 13.5. [Available online at https://ams.confex.com/ams/89annual/techprogram/paper_150417.htm.]

——, L. Zhang, and G. D. Emmitt, 2010: Impact of airborne Doppler wind lidar profiles on numerical simulations of a tropical cyclone. *Geophys. Res. Lett.,* **37,** L05801, doi:10.1029/2009GL041765.

Quinn, P. K., and Coauthors, 2007: Arctic haze: Current trends and knowledge gaps. *Tellus,* **59B,** 99–114.

Reitebuch, O., 2012a: The spaceborne wind lidar mission ADM-Aeolus. *Atmospheric Physics: Background, Methods, Trends,* U. Schumann, Ed., Springer Series on Research Topics in Aerospace, 815–827.

——, 2012b: Wind lidar for atmospheric research. *Atmospheric Physics: Background, Methods, Trends,* U. Schumann, Ed., Springer Series on Research Topics in Aerospace, 487–507.

——, C. Lemmerz, E. Nagel, U. Paffrath, Y. Durand, M. Endemann, F. Fabre, and M. Chaloupy, 2009: The airborne demonstrator for the direct-detection Doppler wind lidar ALADIN on ADM-Aeolus. Part I: Instrument design and comparison to satellite instrument. *J. Atmos. Oceanic Technol.,* **26,** 2501–2515.

Riishojgaard, L. P., Z. Ma, M. Masutani, J. S. Woollen, G. D. Emmitt, S. A. Wood, and S. Greco, 2012: Observation system simulation experiments for a global wind observing sounder. *Geophys. Res. Lett.,* **39,** L17805, doi:10.1029/2012GL051814.

Rothermel, J., and Coauthors, 1998: Remote sensing of multi-level wind fields with high-energy airborne scanning coherent Doppler lidar. *Opt. Express,* **2,** 40–50.

Sawruk, N. W., and Coauthors, 2013: Space qualified laser transmitter for NASA's ICESat-2 mission. *Solid State Lasers XXII: Technology and Devices,* W. A. Clarkson and R. Shori, Eds., International Society for Optical Engineering (SPIE Proceedings, Vol. 8599), 85990O, doi:10.1117/12.2005590.

Schillinger, M., D. Morancais, F. Fabre, and A. Culoma, 2003: ALADIN: The lidar instrument for the Aeolus mission. *Sensors, Systems, and Next-Generation Satellites VI,* H. Fujisada et al., Eds., International Society for Optical Engineering (SPIE Proceedings, Vol. 4881), 40, doi:10.1117/12.463024.

Schwiesow, R. L., and S. D. Mayor, 1995: Coherent optical signal processing for a Doppler lidar using a Michelson interferometer. *Tech. Dig. Ser.–Opt. Soc. Amer.,* **19,** 212–215.

Shaw, G. E., 1995: The Arctic haze phenomenon. *Bull. Amer. Meteor. Soc.,* **76,** 2403–2413.

Siegman, A. E., 1966: The antenna properties of optical heterodyne receivers. *Appl. Opt.,* **5,** 1588–1594.

Simmons, A. J., K. M. Willett, P. D. Jones, P. W. Thorne, and D. P. Dee, 2010: Low-frequency variations in surface atmospheric humidity, temperature, and precipitation: Inferences from reanalyses and monthly gridded observational data sets. *J. Geophys. Res.,* **115,** D01110, doi:10.1029/2009JD012442.

Skamarock, W. C., J. B. Klemp, J. Dudhia, D. O. Gill, D. M. Barker, W. Wang, and J. G. Powers, 2005: A description of the Advanced Research WRF version 2. NCAR Tech. Note NCAR/TN-4681STR, 88 pp.

Stoffelen, A., and Coauthors, 2005: The atmospheric dynamics mission for global wind measurement. *Bull. Amer. Meteor. Soc.,* **86,** 73–87.

——, G.-J. Marseille, F. Bouttier, D. Vasiljevic, S. de Haan, and C. Cardinali, 2006: ADM-Aeolus Doppler wind lidar observation system simulation experiment. *Quart. J. Roy. Meteor. Soc.,* **132,** 1927–1947.

——, ——, J. de Kloe, K. Houchi, H. Körnich, and N. Žagar, 2008: Scientific preparations for Aeolus and Aeolus follow-on. *Ninth Int. Winds Workshop,* Annapolis, MD, EUMETSAT, 8 pp. [Available online at www.knmi.nl/publications/fulltexts/dwl_9iww.pdf.]

Tan, D. G. H., E. Andersson, M. Fisher, and L. Isaksen, 2007: Observing system impact assessment using a data assimilation ensemble technique: Application to the ADM-Aeolus wind profiling mission. *Quart. J. Roy. Meteor. Soc.,* **133,** 381–390.

Trenberth, K. E., 1997: Using atmospheric budgets as a constraint on surface fluxes. *J. Climate,* **10,** 2796–2809.

Tucker, S. C., C. J. Senff, A. M. Weickmann, W. A. Brewer, R. M. Banta, S. P. Sandberg, D. C. Law, and R. M. Hardesty, 2009: Doppler lidar estimation of mixing height using turbulence, shear, and aerosol profiles. *J. Atmos. Oceanic Technol.,* **26,** 673–688.

——, C. Grund, T. Delker, M. Adkins, B. Good, P. Kaptchen, and D. Gleeson, 2012: Wind profiling with the optical autocovariance wind lidar: Results of validation testing. *Second Conf. on Transition of Research to Operations: Successes, Plans, and Challenges,* New Orleans, LA, Amer. Meteor. Soc., TJ10.2. [Available online at https://ams.confex.com/ams/92Annual/webprogram/Paper202733.html.]

Uppala, S. M., and Coauthors, 2005: The ERA-40 Re-Analysis. *Quart. J. Roy. Meteor. Soc.,* **131**, 2961–3012.

Vecchi, G. A., B. J. Soden, A. T. Wittenberg, I. M. Held, A. Leetmaa, and M. J. Harrison, 2006: Weakening of tropical Pacific atmospheric circulation due to anthropogenic forcing. *Nature*, **441**, 73–76.

Vermeesch, K., B. Gentry, G. Koch, M. Boquet, H. Chen, U. Singh, B. Demoz, and T. Bacha, 2011: Comparison of wind measurements at the Howard University Beltsville Research Campus. Preprints, *Fifth Symp. on Lidar Atmospheric Applications,* Seattle, WA, 4.4. [Available online at https://ams.confex.com/ams/91Annual/webprogram/Paper181653.html.]

Wagener, T. J., N. Demma, J. D. Kmetec, and T. S. Kubo, 1995: 2-mm lidar for laser-based remote sensing: Flight demonstration and application survey. *IEEE Aerosp. Electron. Syst. Mag.,* **10,** 23–28.

Weimer, C., R. Schwiesow, and M. LaPole, 2004: CALIPSO: Lidar and Wide-field camera performance. *Earth Observing Systems IX,* W. L. Barnes and J. J. Butler, Eds., International Society for Optical Engineering (SPIE Proceedings, Vol. 5542), 74, doi:10.1117/12.561613.

Weissmann, M., and C. Cardinali, 2007: Impact of airborne Doppler lidar observations on ECMWF forecasts. *Quart. J. Roy. Meteor. Soc.,* **133,** 107–116.

——, R. Busen, A. Dörnbrack, S. Rahm, and O. Reitebuch, 2005: Targeted observations with an airborne wind lidar. *J. Atmos. Oceanic Technol.,* **22,** 1706–1719.

——, R. H. Langland, C. Cardinali, P. M. Pauley, and S. Rahm, 2012: Influence of airborne Doppler wind lidar profiles near Typhoon Sinlaku on ECMWF and NOGAPS forecasts. *Quart. J. Roy. Meteor. Soc.,* **138,** 118–130.

Werner, C., 2004: Doppler wind lidar. *Lidar: Range-Resolved Optical Remote Sensing of the Atmosphere,* C. Weitkamp, Ed., Springer Series in Optical Sciences, Vol. 102, Springer, 325–354.

Winker, D. M., J. Pelon, and M. P. McCormick, 2003: The CALIPSO mission: Spaceborne lidar for obervation of aerosols and clouds. Lidar Remote Sensing for Industry and Environment Monitoring III, U. N. Singh, T. Itabe, and Z. Lui, Eds., International Society for Optical Engineering (SPIE Proceedings, Vol. 4893), 1–11.

——, W. H. Hunt, and M. J. McGill, 2007: Initial performance assessment of CALIOP. *Geophys. Res. Lett.,* **34,** L19803, doi:10.1029/2007GL030135.

Wood, S. A., Jr., G. D. Emmitt, and S. Greco, 2000: DLSM: A coherent and direct detection lidar simulation model for simulating space-based and aircraft-based lidar winds. *Laser Radar Technology and Applications V,* G. W. Kamerman et al., Eds., International Society for Optical Engineering (SPIE Proceedings, Vol. 4035), 2, doi:10.1117/12.397788.

WMO, 1996: Guide to meteorological instruments and methods of observation. 6th ed. WMO-8, 681 pp.

——, cited 2012a: Statement of Guidance for Global Numerical Weather Prediction (NWP). [Available online at www.wmo.int/pages/prog/www/OSY/GOS-RRR.html.]

——, 2012b: WIGOS: WMO Integrated Global Observing System; Final report of the Fifth WMO Workshop on the Impact of Various Observing Systems on Numerical Weather Prediction. WMO Tech. Rep. 2012-1, 23 pp.

Yang, X.-Y., J. C. Fyfe, G. M. Flato, 2010: The role of poleward energy transport in Arctic temperature evolution. *Geophys. Res. Lett.,* **37,** L14803, doi:10.1029/2010GL043934.

Žagar, N., N. Gustafsson, and E. Källén, 2004: Dynamical response of equatorial waves in four-dimensional variational data assimilation. *Tellus,* **56A**, 29–46.

——, A. Stoffelen, G.-J. Marseille, C. Accadia, and P. Schlüssel, 2008: Impact assessment of simulated Doppler wind lidars with a multivariate variational assimilation in the tropics. *Mon. Wea. Rev.,* **136,** 2443–2460.

Zhang, L., and Z. Pu, 2010: An observing system simulation experiment (OSSE) to assess the impact of Doppler wind lidar (DWL) measurements on the numerical simulation of a tropical cyclone. *Adv. Meteor.,* **2010,** 743863, doi:10.1155/2010/743863.